JVSTA
JOURNAL OF VACUUM SCIENCE AND TECHNOLOGY A

Critical review: Effects of complex interactions on structure and dynamics of supported metal catalysts

Anatoly I. Frenkel, Michael W. Cason, Annika Elsen, Ulrich Jung, Matthew W. Small et al.

Citation: J. Vac. Sci. Technol. A **32**, 020801 (2014); doi: 10.1116/1.4820493
View online: http://dx.doi.org/10.1116/1.4820493
View Table of Contents: http://avspublications.org/resource/1/JVTAD6/v32/i2
Published by the AVS: Science & Technology of Materials, Interfaces, and Processing

REVIEW ARTICLE

Critical review: Effects of complex interactions on structure and dynamics of supported metal catalysts

Anatoly I. Frenkel[a)]
Physics Department, Yeshiva University, New York, New York 10016

Michael W. Cason, Annika Elsen, Ulrich Jung, Matthew W. Small, and Ralph G. Nuzzo
Department of Chemistry, University of Illinois Urbana-Champaign, Urbana, Illinois 61801

Fernando D. Vila and John J. Rehr
Department of Physics, University of Washington, Seattle, Washington 98195

Eric A. Stach
Center for Functional Nanomaterials, Brookhaven National Laboratory, Upton, New York 11973

Judith C. Yang
Department of Chemical and Petroleum Engineering, University of Pittsburgh, Pittsburgh, Pennsylvania 15261

(Received 7 June 2013; accepted 23 August 2013; published 18 September 2013)

This review article takes a new look at the problem of characterization of structural properties and reaction dynamics of supported metal catalysts. Such catalysts exhibit an inherent complexity, particularly due to interactions with the support and the adsorbate molecules, which can be highly sensitive to environmental conditions such as pressure and temperature. Recent reports demonstrate that finite size effects such as negative thermal expansion and large bond length disorder are directly caused by these complex interactions. To uncover the atomistic features underlying the reaction mechanisms and kinetics of metal catalysts, experimental characterization must accommodate the challenging operation conditions of catalytic processes and provide insights into system attributes. The combined application of x-ray absorption spectroscopy (XAS) and transmission electron microscopy (TEM) for this type of investigations will be examined, and the individual strengths and limitations of these methods will be discussed. Furthermore, spatial and temporal heterogeneities that describe real catalytic systems and can hinder their investigation by either averaging (such as XAS) or local (such as TEM) techniques alone will be addressed by conjoined, multiscale, *ab initio* density functional theory/molecular dynamics modeling of metal catalysts that can both support and guide experimental studies. When taken together, a new analysis scheme emerges, in which different forms of structure and dynamics can be fully characterized by combining information obtained experimentally by *in situ* XAS and electron microscopy as well as theoretically via modeling. © *2014 American Vacuum Society*. [http://dx.doi.org/10.1116/1.4820493]

I. INTRODUCTION

A. Historical development of catalysis

Catalysis is ubiquitous in nature.[1] One of the earliest examples of catalytical reactions known to humans is the fermentation of sugar to ethanol. Records of brewing by the Sumerians are about 6000 years old.[2] The first systematic studies of catalytically active substances, however, were not carried out until the beginning 19th century,[3–5] leading ultimately to the fundamental definition of the concept of catalysis by Berzelius in 1835.[6] The later 19th and earlier 20th century saw tremendous advances in understanding fundamental chemical reaction kinetics. Several examples of progression in this vein have to be mentioned. These include: The quantitative analysis of reaction rates by Wilhelmy in 1850,[7] the law of mass action by Guldberg and Waage in 1864,[8] the description of the temperature dependence of reaction rates by Arrhenius in 1889,[9] the steady state approximation by Chapman in 1913,[10] the quantitative theory of adsorption of gases on surfaces by Langmuir in 1915,[11] the kinetic mechanism of reactions in heterogeneous catalysis by Hinshelwood in 1927,[12] and the transition-state theory of chemical reaction dynamics by Eyring *et al.* in 1935.[13] These findings facilitated the concomitant development of various novel kinds of catalysts for industrial applications. Notable examples include the hydrogenation of fats [Sabatier, 1897 (Ref. 14)], the ammonia synthesis [Haber, 1909 (Refs. 15 and 16)], and the synthesis of hydrocarbons from coal-derived water gas [Fischer and Tropsch in the 1920s (Ref. 17)]. In the following decades, the industrial

a)Electronic mail: anatoly.frenkel@yu.edu

applications of catalysts grew enormously, mainly driven by the demands of the oil and later the plastics industry.[18,19] A prominent example is the synthesis of polymers from olefins [Ziegler and Natta in the early 1950s (Ref. 20)]. During the late 20th century up to the present times, the progress, aside from the development of novel catalysts, has mainly been driven by efforts to enhance the efficiency, selectivity, and sustainability of existing catalytic materials. An important example of such so-called "environmental" or "green catalysts" is the three-way catalyst[21,22] that is used for the removal of the pollutants CO, NO, and hydrocarbons from automobile exhaust. Nowadays, nearly all chemical processes (i.e., 85–90%) used in industry (e.g., for the production of plastics, synthetic fibers, dyes, crop-protection agents, and pharmaceuticals) are based on some form of catalysis.[19,23]

B. Structure and dynamics of supported metal catalysts

Supported metal catalysts exhibit pronounced structural flexibility, chemical reactivity, selectivity, and stability.[24] Unfortunately, these systems are typically only poorly characterized in terms of the fundamental structural and dynamical properties (so-called descriptors) that determine their overall catalytic performance. Structural properties comprise size, shape, defects (e.g., edges, corners, faceting, twinning), and chemical composition (e.g., bi-, multicomponent, and alloy nanoparticles; catalytic promoters and poisons) of the nanoparticles and the support.[25] Dynamical aspects include interactions between the nanoparticles, the support, and the adsorbate molecules, which can be sensitively pressure- and temperature-dependent.[26] Examples are electronic interactions/chemical bonding between the nanoparticles and the support (e.g., order,[27] nanoparticle shape[28–30]) as well as adsorption, surface diffusion, and reactions of the adsorbates on both the nanoparticles[26,31] and the support[31–35] (e.g., steric effects, coverage changes,[26] different reactivity of specific adsorption sites,[36] spillover of adsorbates onto the support[37]). Because of the inherent complexity of supported catalysts, it is important both to improve understanding of the fundamental processes that occur on the atomic/molecular level as well as the parameters that most fundamentally control reaction rates and selectivity.[38,39] The fact that many parameters and their complex interactions are responsible for the reactivity of metal nanoparticles stands as one main distinction to biocatalysts, i.e., enzymes, for which the dynamics of a single catalytically active site is most commonly involved in mediating rate enhancements.

Efforts in understanding the interplay of structural properties and reaction dynamics are led by the use of "model systems." In particular, two kinds of model systems have been intensively investigated: structurally well-defined single crystals[40] and ligand-capped/supported metal catalysts prepared by elaborate means of chemical synthesis.[41] Single crystals (mainly metals) have been predominantly studied under ultrahigh vacuum (UHV) conditions. The pioneering work by the groups of Ertl[42–44] and Somorjai[45–47] has been particularly influential in this domain. A notable example is the discovery that some important classes of reactions only occur at specific structural sites, such as kinks or step edges.[48] Unfortunately, translation of findings obtained for well-defined single crystals in UHV to real supported catalysts under operating conditions (i.e., in gas atmospheres of variable pressures and temperatures) is not always possible. The discrepancies between the structural and environmental attributes between real catalysts and the different kinds of model systems also have been referred to as "material" or "pressure gap."[49,50]

Understanding the interplay of complex interactions in catalysis is challenging, in part, because of effects arising from the finite sizes of the nanoparticles. Scaling laws apply for many structural and dynamic features of finite systems except for dimensions below 1–5 nm.[51–53] For larger particles, physical or chemical attributes $\chi(n)$ depend monotonically on the number of the constituents n: $\chi(n) = \chi(\infty) + An^{-\beta}$, where A is a constant and β is a positive exponent.[52] For smaller particles, these features display a markedly nonmonotonic behavior (Fig. 1). The latter view of structure/property correlations is supported by a large amount of experimental data[54–58] and theoretical calculations.[59–62]

It has been noted in past work that the kinetic properties of reactions of supported metal nanoparticle catalysts are nonequilibrium[63,64] and couple dynamical underpinnings over multiple time scales.[65] The time scales of the fundamental steps in catalytic reaction mechanisms—adsorption, surface diffusion, reactions, and desorption—are often shorter than 10^{-3} s. The time scale of adsorbate vibrations is in the order of 10^{-12} s, those of electronic reconfiguration (e.g., electronic excitations, bond breaking) in the order of 10^{-15} s. These processes, occurring at different time scales, obey different physical laws and, perhaps most challenging, require different methods to determine the nature of their coupling and effects on specific features of reactivity.

Despite the progress made in understanding the reactivity of catalysts, almost every observation is justified *ex post facto*. These justifications either use or build upon a set of

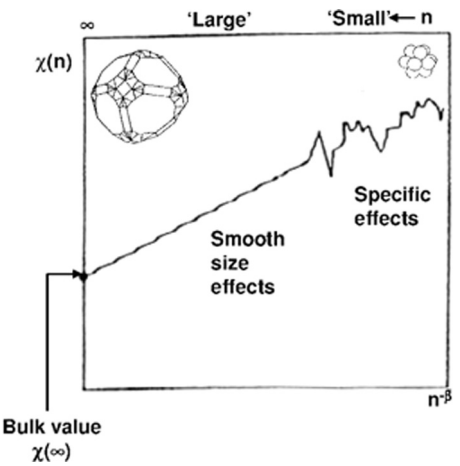

FIG. 1. Cluster size dependence of a cluster property $\chi(n)$ on the number n of cluster constituents. The data are plotted vs $n^{-\beta}$, where $\beta \geq 0$ is a system-specific parameter. Reprinted with permission from Jortner and Rao, Pure Appl. Chem. **74**, 1491 (2002). Copyright 2002, IUPAC.

common characteristics of the system—the descriptors, *vide supra*—that describe what properties of the catalyst either facilitate or inhibit the reaction. For example, a descriptor commonly used for characterization of electrocatalysts and bimetallic alloys is the d-band center.[66] It is also possible to outline descriptors that have a more direct bearing on the reaction kinetics such as transition state geometries and activation energies. While the dominant factors defining catalytic activity and selectivity of a given system can be better understood with the help of catalytic descriptors, the goal of a rational catalyst design remains largely an unrealized challenge.[67] So, although a deep understanding of catalytic systems has been accumulated and reasonable predictions of catalyst properties that may favor a given reaction are possible, the ability to specifically "tailor" the atomic structure of a catalyst to perform a desired reaction remains extremely limited.

C. Catalysts characterization

Because of its inherent complexity, the characterization of supported metal catalysts requires the use of multiple, complementary experimental techniques to elucidate their nature as it exists under operating conditions to give a combined, self-consistent picture. In particular, it has been demonstrated in several earlier studies that results obtained under operation conditions can differ quite significantly from those evidenced in static pre- or post-reaction measurements.[68–70] The most frequently used *in situ* or *in operando* methodologies are based on scattering or spectroscopy, including XRD,[71–73] x-ray absorption spectroscopy (XAS) [x-ray absorption near-edge structure (XANES) and extended x-ray absorption fine structure (EXAFS)],[72,73] XPS,[74] Auger spectroscopy,[75] Mößbauer spectroscopy,[76] magnetic resonance (ESR and NMR),[77,78] UV/VIS spectroscopy,[79,80] vibrational spectroscopy (IR and Raman spectroscopy),[80,81] and thermal desorption spectroscopy.[82] While very powerful, each of these methods typically yields ensemble average information, which may provide only incomplete or even incorrect information in terms of the underlying structural properties and reaction dynamics. XAS is a particularly widely used *in situ* technique because it can easily be applied in various kinds of environments, exhibits a high temporal resolution [e.g., Quick EXAFS, QEXAFS (Ref. 83)], and establishes comprehensive information about structural and electronic properties.[84–87] With local probes, such as (S)TEM, AFM, or STM, it also is possible to determine structural features, such as size, shape, and defects of individual nanoparticles. In the majority of cases, they cannot easily be applied for studies under chemically harsh operating conditions. One interesting exception is the environmental TEM/STEM, which can be used for *in operando* studies with atomic resolution in gaseous or liquid atmospheres at pressures up to $\sim$1 atm.[88–92]

Another approach with considerable promise to improve characterization is the combination of experiment and theory into a unified multi-technique analysis scheme, as has been well-described by Billinge and Levin.[93] The recent advances in theoretical modeling of catalytic mechanisms,[94–96] notwithstanding the extension of computational methods, confront significant challenges, most notably, the required computing power (and time) needed to accurately model a system of appreciable size at the quantum level. Another, somewhat less acknowledged limitation, is that the predictive power of computational methods is still improving. Indeed, one of the better-known conundrums that illustrate this aspect is the nature of the preferred binding site of CO on Pt(111).[97–99] It was not until 2002 that the reason (i.e., the poor treatment of the CO electronic structure and bond breaking[100]) for the incorrect prediction of CO favoring a three-fold binding site instead of a top binding site on Pt(111) was found. So, while computational results offer a useful means of interpreting and predicting results, they are far from an unambiguous determination of the efficiency of a catalyst. Multi-technique characterization is a powerful next step toward better understanding of catalytic reaction mechanisms, but its predictions will remain limited if the correlated experiments are not performed in ways that can accommodate demanding conditions.[101–104]

D. Scope of the review

Progress in developing methods for understanding how catalysts behave has advanced along many avenues. In the following sections, the state of the art for some of the most powerful catalysis characterization techniques will be highlighted. Specifically, density functional theory (DFT) and molecular dynamics (MD) have been recently combined with theoretical calculations of x-ray spectra to explain dynamic structure changes in supported metal nanoparticles and the complex condition-dependent interactions that occur with the support and adsorbates. Theory is well-suited to model the effects in the nanoparticle-support interface of heterogeneous catalysts in response to the changes in temperature and pressure. Progress in XAS-based methods is particularly relevant, as they are the perhaps most-intensively used by the catalysis community, due to the capability they provide to monitor reactions with high temporal resolution at relevant temperatures and pressures. This will be illustrated using several exemplary cases in which the atomic and electronic structures of catalysts evolve with changing environmental conditions. We will then discuss correlated TEM measurements that illustrate the integration of single-particle, atomic-resolution imaging with ensemble-average methods. We will discuss requirements for correlating multiple experiments (local and average ones) *in situ* and *in operando* on the same system, using a portable reactor cell approach. Finally, emerging new opportunities that will rely on the interpretation of experimental and theoretical data obtained on the same multicomponent system will be explored.

II. X-RAY ABSORPTION SPECTROSCOPY

A. Introduction

XAS is among the best techniques for comprehensive investigations of finite size effects and their influence on the

catalytic activity of nanocatalysts. With this method, fine structure in the resonance region of the x-ray absorption coefficient (called the absorption edge) is measured in either a transmission or fluorescence detection mode (Fig. 2). The edge region (within 30 eV below to 40 eV above the edge), known as the XANES, contains information about the electronic structure and local geometry of the absorbing atom and its nearest neighbors. The post-edge region that extends from ~40 eV to between 1000 and 1500 eV (depending on the system) past the edge contains an oscillatory signal and is known as the extended EXAFS.[105] The origin of the fine structure is the interference between the incoming and scattered photoelectron waves. The interference pattern contains quantitative information about the local atomic environment in the proximity of the absorbing atom. The frequency of these oscillations can be quantitatively related to the distances between the absorbing atom and atoms within a given coordination shell around it. The EXAFS signal therefore contains information about interatomic distances and their disorder (due to the static and dynamic displacements of all atoms from their average positions). The amplitude of these oscillations correlates with the number of neighboring atoms of a given type.

The oscillatory part of the absorption coefficient—$\chi(k)$—contains the sum of all contributions $\chi_i(k)$ from groups of neighbor atoms at approximately equal distances from the absorbing atoms (i.e., within the ith shell), which are often written as[106]

$$\chi_i(k) = \frac{S_0^2 n_i}{kR_i^2} |f_i^{\text{eff}}(k)| \sin\left[2kR_i - \frac{4}{3}\sigma_i^{(3)}k^3 + \delta_i(k)\right] \times e^{-2\sigma_i^2 k^2} e^{-2R_i/\lambda_i(k)}, \quad (1)$$

where k is the photoelectron wave number, $f_i^{\text{eff}}(k)$ and $\delta_i(k)$ are the photoelectron scattering-path amplitude and phase, respectively, S_0^2 is the passive electron reduction factor, n_i is the degeneracy of the scattering path, R_i is the effective half-path length (which equals the interatomic distance for single scattering paths), σ_i^2 is the mean-square deviation in R_i, $\sigma_i^{(3)}$ is the third cumulant of the pair distribution function,[107] and $\lambda_i(k)$ is the photoelectron mean free path. The most dominant contribution to the EXAFS signal originates from backscattering of the photoelectron by neighboring atoms toward the absorbing atom ("single scattering"). More complex scattering patterns involve the electron wave's reflections by multiple atoms.[108] This multiple scattering approach is essential in order to accurately calculate the absorption coefficient. For example, the contribution from multiple scattering by atoms along an atomic row, known as the shadowing or focusing effect, can dominate the backscattering. The amplitude reduction factor S_0^2 describes the intrinsic losses upon excitation, which arise due to the many-body effects during the photoabsorption process. The scattering amplitudes and phases, along with the photoelectron mean free paths for different scattering configurations contributing to the EXAFS signal, are calculated *ab initio*. Among the most widely used software programs for these calculations are FEFF [versions 6,[106] 8,[109] and 9 (Ref. 110)], EXCURVE,[111] and GNXAS.[112]

Due to the relatively large penetration depth of hard x-rays (tens of micrometers), many reactors are available for *in situ* and *operando* studies in gases and liquids, electrochemical or fuel cell studies, and even ones for high pressure and temperature conditions.[73,113–121] High brilliance third-generation synchrotron sources further enable the investigation of low concentrations of catalysts and the use of sub-micron x-ray beams for spatially resolved XANES and EXAFS measurements. Another important characteristic of synchrotron XAS experiments is the extremely short (10^{-15}–10^{-16} s) lifetime involved in x-ray absorption. For this reason, XANES and EXAFS are found in many studies and applications that require a high temporal resolution.[122]

For an extended description of different aspects of XAS methodology, the interested reader is referred to several useful books, book chapters, and review articles.[108,123–127] Detailed discussion of specialized methods suitable for the characterization of nanoparticle size, shape, and atomic structure, based on multiple scattering analysis of EXAFS data, have also been recently reported.[118,128–132] Also of interest are several recent reviews outlining XAS-based applications to structural and catalytic studies of nanomaterials.[133–136]

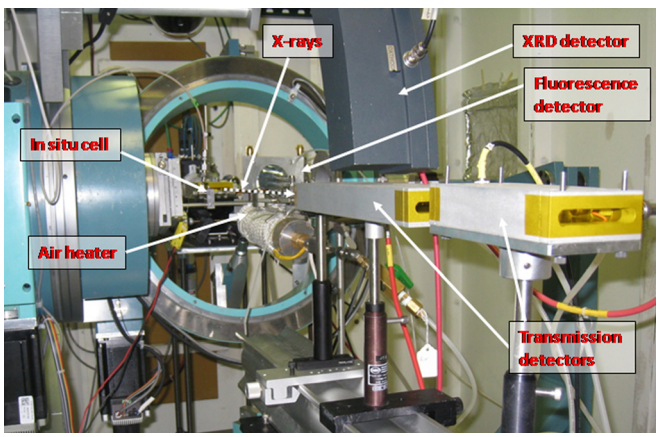

FIG. 2. (Color online) X-ray absorption spectroscopy setup at beamline X18A at the National Synchrotron Light Source (Brookhaven National Laboratory).

B. Complex interactions between catalysts structure and dynamics

The most intriguing feature of nanomaterials is the prospects they engender for mesoscopic forms of complexity—where physicochemical properties exhibit important or useful pertubations that arise as a consequence of their finite size. Pertubations can be quite pronounced and XAS provides an extremely useful method for exploring such phenomena. An example for finite size effects of nanoparticles on XANES and EXAFS data is shown in Fig. 3. The edge region in the x-ray absorption coefficient [Fig. 3(a)] of Pt nanoparticles on γ-Al_2O_3 support (measured under 2.5% CO/97.5% He flow at room temperature) demonstrates broadening of the peak region near the absorption maximum (known as "white line") relative to bulk Pt. This effect is due to both the nanometer size of the particles and the charge

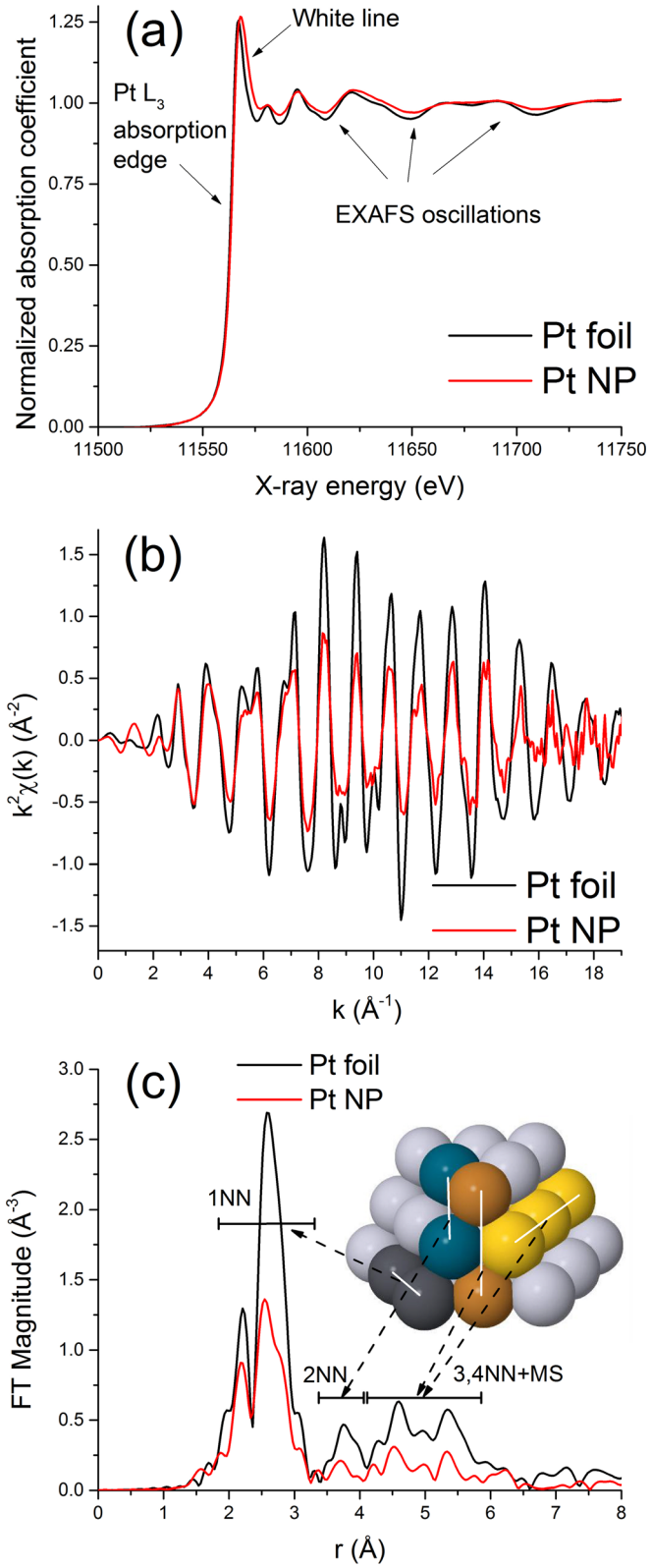

FIG. 3. (Color online) Raw EXAFS data for Pt nanoparticles supported on high surface area γ-Al_2O_3 substrate and bulk Pt (a) in energy, (b) in k-space, and (c) in r-space. The inset in (c) shows a model of a truncated cuboctahedral cluster and different groups of atomic arrangements that contribute to different peaks in r-space.

exchange between the Pt and adsorbed CO. These effects are pronounced in this case due to high portion of surface and interface sites occupied by Pt atoms in particles of this size. The data in Fig. 3(b) illustrate the effect of both the coordination number and the disorder on EXAFS oscillations that are dampened as compared to bulk Pt. Figure 3(c) shows the magnitude of the Fourier transform of the EXAFS oscillations for the nanoparticles and the bulk data. The peak positions are uncorrected for the photoelectron phase shift [Eq. (1)] and are thus shifted to lower distances relative to the real space values. The peak positions correlate with the pair distribution function peaks that correspond to the 1st, 2nd, 3rd, etc., coordination shells, although for higher order shells such determination is difficult due to the contribution of multiple scattering paths in the same r-range as single scattering paths of the same length [Fig. 3(c)].

XAS methods not only possess the required accuracy to detect finite size effects in nanomaterials, but can also illuminate the nature of the complex interactions of the components and their environment. One illustration of this is seen in a recent study of a Pt catalyst supported on both high surface area γ-Al_2O_3 and carbon substrates that revealed several aspects of anomalous behavior.[31,32] For example, γ-Al_2O_3-supported Pt particles of 1 nm average diameter demonstrated the following attributes: (1) an unexpected negative thermal expansion (NTE), revealed in the bond length contraction at elevated temperatures [Fig. 4(a)], (2) size-dependent changes in the static disorder, revealed by the large y-intercept values linearly interpolated for the mean square displacement of Pt-Pt distances [Fig. 4(b)], and (3) shifting of the onset of the Pt L_3 absorption edge to lower energies with increasing temperature [Fig. 4(c)]. These findings demonstrate that the effects of substrate and adsorbates on the thermodynamic properties of metal nanoparticles are as important as the particle size, which has long been believed to be a dominant factor responsible for non-bulk-like properties (e.g., decrease of lattice parameters of small clusters compared to the bulk,[137–139] or size-dependent changes in vibrational dynamics[139–143]). These results[31] show that the effects of the size, support, and atmosphere on the structural (Fig. 4), dynamic (Fig. 5), and electronic (Fig. 6) properties are comparable. This highlights a need for new experimental and theoretical methodologies that are able to capture the details of substrate and adsorbate influences on the thermodynamic properties of the metal clusters in addition to details of cluster size, structure, and shape. An important requirement for such methods is that they are suited to measure all of these attributes for catalytic processes *in situ*, while controlling pressure and temperature.

A recent illustration of this approach is the work by Small *et al.*,[26] where the effect of gas concentration, pressure, and temperature on adsorbate coverage, structure, shape, and electronic state of Pt clusters supported on γ-Al_2O_3 were measured. The data in this study show that these effects can be modeled as arising from separable components (Fig. 7). For example, coordination numbers and bond length disorder were found to strongly correlate with adsorbate coverage and temperature. The γ-Al_2O_3-supported particles exhibited enhanced static disorder (and thus strain) at increased partial pressure (and thus coverage) of CO. An opposite trend was seen in a H_2 atmosphere. Furthermore, the metal–metal coordination numbers increased at high temperature under CO

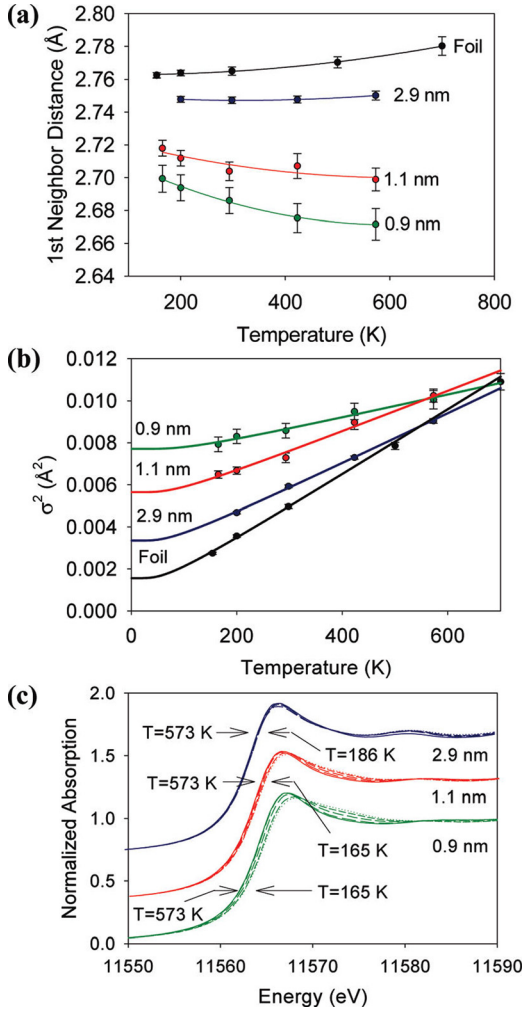

FIG. 4. (Color online) Effects of the average particle size on the Pt-Pt bond length (a), mean square disorder (b) and near-edge region (c) for γ-Al_2O_3-supported Pt nanoparticles under He flow. Adapted with permission from Sanchez *et al.*, J. Am. Chem. Soc. **131**, 7040 (2009). Copyright 2009, American Chemical Society.

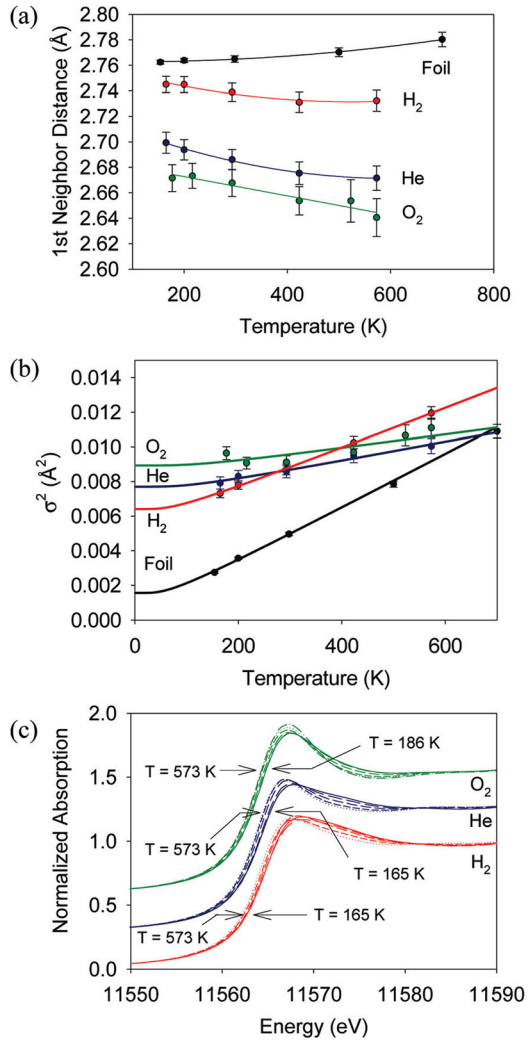

FIG. 5. (Color online) Effects of the atmosphere (H_2, He or O_2) on the Pt-Pt bond length (a), mean square disorder (b), and near edge region (c) for γ-Al_2O_3-supported Pt nanoparticles with an average size of 0.9 nm. Adapted with permission from Sanchez *et al.*, J. Am. Chem. Soc. **131**, 7040 (2009). Copyright 2009, American Chemical Society.

(at all partial pressures), indicating adsorbate-induced restructuring.[144] These effects are shown schematically in Fig. 8. By independently varying the partial pressure of the gas and the system's temperature, this study revealed how the complex structural and electronic properties of this important—and representative—heterogeneous catalyst evolve under varying conditions. Specifically, it is found that CO elicits strong structural and electronic changes of the Pt nanoparticles, while H_2 adsorption mainly acts to relieve significant metal-metal bond strains. The XANES data (Fig. 9) indicated a series of contributions that were ascribed to particle-adsorbate, particle-support, and adsorbate-support interactions. The intertwining of these different contributions could be related to the patterns of condition-dependent charge exchange, which in turn mediate the catalysts' atomic and electronic structure (Fig. 7)

$$S(T,P) = \frac{A}{\alpha(P)e^{-n/T} + 1} + BT + C(P). \quad (2)$$

The first term in the right-hand side of Eq. (2) describes the metal–adsorbate interactions via the (P,T)-dependent adsorbate coverage, the second term the contribution of the metal–support interaction, and the last term the adsorbate–support interaction. These data also show that charge exchange due to metal–support interactions (affecting the slope of the signals shown in Fig. 9) is a dominant factor in the electronic structure changes observed for the working catalyst. The nature of this interaction in oxide supported metal clusters is discussed in the theory section below.

III. THEORETICAL MODELING

A. Introduction

The nature of atomic and electronic structure at the nanoscale is of both fundamental and technological importance.[145,146] This regime is especially relevant to the problem of understanding the structure and function of supported nanoscale catalysts. This problem is challenging for many reasons. In particular, nanoscale structural properties differ significantly from those of bulk condensed matter or

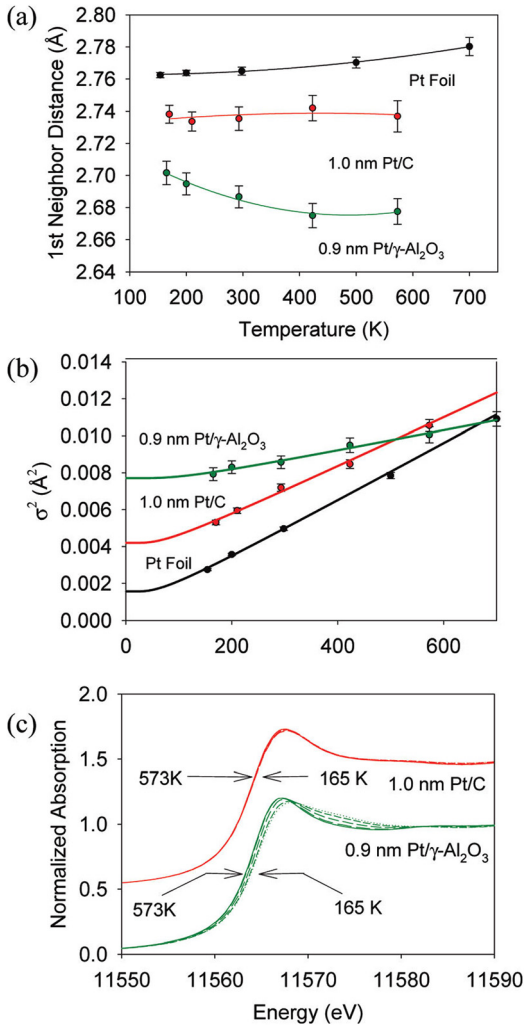

FIG. 6. (Color online) Effects of the support (γ-Al_2O_3 or C) on the Pt-Pt bond length (a), mean square disorder (b), and near-edge region (c) for γ-Al_2O_3-supported Pt nanoparticles of similar average sizes (0.9 and 1.0 nm) and under He flow. Adapted with permission from Sanchez *et al.*, J. Am. Chem. Soc. **131**, 7040 (2009). Copyright 2009, American Chemical Society.

solid surfaces[147,148] and can be difficult to probe with current experimental techniques. XAS has played an important role in elucidating such properties, since it is an element-specific probe of atomic-scale short range order. For example, XAS

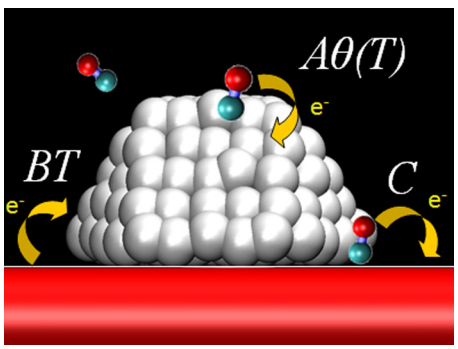

FIG. 7. (Color online) Effects of adsorbate-metal, support-metal, and adsorbate-support interactions on the charge state of supported metal nanoparticle. Reprinted with permission Small *et al.*, ACS Nano **6**, 5583 (2012). Copyright 2011, American Chemical Society.

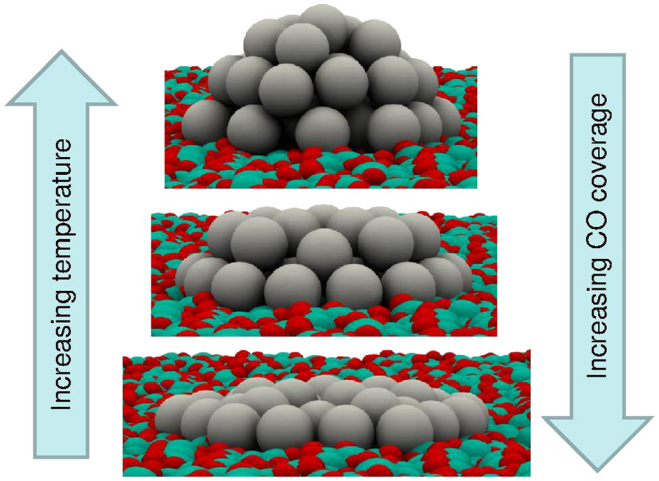

FIG. 8. (Color online) Schematics of the effects of metal-adsorbate interactions on the shape of supported metal particles (see Ref. 26 for details).

probes of supported nanoscale Pt clusters have revealed many unusual properties, as described above. Specifically, it has been shown in XAS studies that small $Pt_{5\text{-}25}$ nanoparticles supported on γ-Al_2O_3 are highly disordered, with measured mean square relative displacements of the Pt-Pt bonds up to four times larger than those in the bulk metal. In addition, the supported clusters show thermal contraction of the nearest-neighbor Pt-Pt distances with increasing temperature (i.e., a NTE).[31,32]

Substrate effects are particularly important in understanding their behavior, and have been covered extensively in the surface science literature.[149] These treatments, however, generally assume equilibrium properties with time-independent potential energy surfaces. Less appreciated is the observation[150,151] that even if the full system (nanoparticle plus support) is in thermal equilibrium, nanoscale properties can exhibit substantial fluctuations with respect to equilibrium which are dynamically varying over multiple time scales, as discussed further below. Thus, the potential energy surface of the nanoparticle can be time-dependent due to dynamic coupling to the support. This interpretation has led to a model of supported catalysts picturesquely dubbed "Shake-Rattle-and-Roll,"[152] which can explain many of these anomalous properties. In addition to bond vibrations (i.e., *shaking*) involving THz frequencies, supported nanoscale systems are tethered to surface bonding sites and hence their center of mass tends to librate. This induces a stochastic *rattle* motion, typically at sub-THz frequencies. At significantly longer time scales (tens of ps) surface bonds tend to break, and the clusters can *roll* to new positions on the substrate. The combined motion of many such nanosystems eventually leads to particle sintering. Figure 10 illustrates these dynamical regimes for Pt_{10} nanoparticles on γ-Al_2O_3.

These temperature-induced structural changes are correlated with changes in the electronic structure of the clusters. XANES measurements (Fig. 11) of the L_3 edge of Pt show a clear red shift of the edge with increasing temperatures, together with an increase in white line intensity. Figure 11 also shows theoretical spectra obtained by sampling of multiple

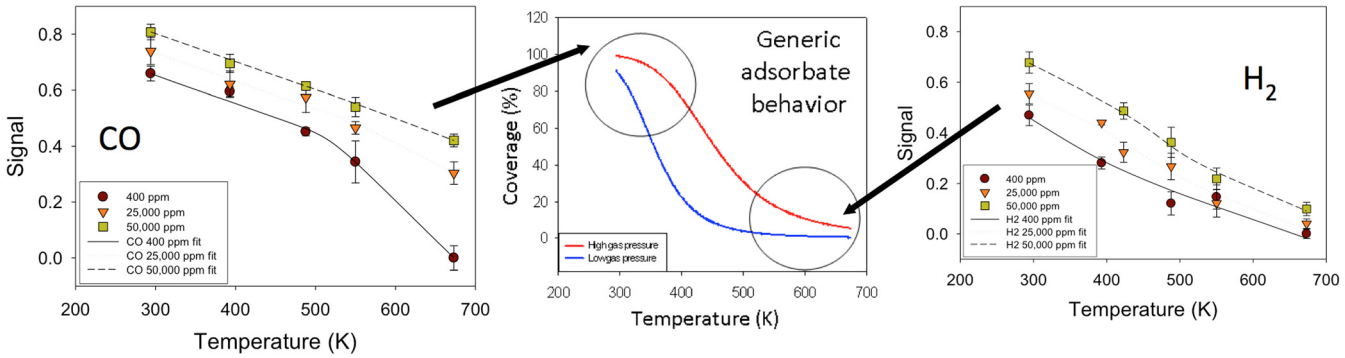

FIG. 9. (Color online) Effects of the adsorbate partial pressure on the integrated area ("Signal") under the ΔXANES data (obtained by subtracting the 673 K data from that of the actual temperatures). The signal shows a strong dependence on pressure and temperature, in qualitative agreement with theoretical expectations [Eq. (2)]. Reprinted with permission Small *et al.*, ACS Nano **6**, 5583 (2012). Copyright 2011, American Chemical Society.

conformations from DFT/MD trajectories (*vide infra*).[150] The error bars in the theoretical curves depict the standard deviations of the spectra due to dynamical disorder. The effect is particularly large at the white line, indicating that exhaustive conformational sampling is required to reproduce the experimental results.

These remarkable observations provide a motivation to reinvestigate the behavior of supported catalysts from a dynamic perspective. Although considerable progress has been made to date, this investigation is far from complete. For example, the effects of dynamics on reaction rates have yet to be fully explored. Nevertheless, the results so far offer tantalizing new insights into nanoscale behavior including possible dynamic mechanisms for catalysis.

B. Theoretical models

Here we briefly review several theoretical approaches for understanding supported Pt clusters. There have been many advances in the understanding of nanoscale structures in recent years. These advances have been driven partly by theoretical developments in nano- and surface science, and partly by the enormous increase in computer power and the efficiency of computational methods. For example, DFT and *ab initio* electronic structure methods have enabled semiquantitative calculations of many physical properties of such nanoscale systems. The use of DFT/MD simulations[153] that employ *ab initio* DFT potentials is crucial, since classical model potentials in conventional MD are not sufficiently flexible to capture dynamical charge-transfer, bond-breaking, and other nonequilibrium effects. As discussed in the previous section, such computer simulations often reveal unexpected insights into both structure and reactivity. Moreover, modern DFT methods also enable multiscale modeling of supported nanostructures.[154]

Conventional analysis methods are based on a Boltzmann distribution of various equilibrium conformations.[155,156] However, such methods can become computationally intractable to treat these unusual nanoscale phenomena, especially for very large nanoparticles. An attractive alternative approach is provided by *ab initio* finite-temperature DFT/MD calculations.[153,157] These methods can provide a detailed understanding of the atomistic behavior and dynamics of the nanoparticles. For example, simulations for prototypical Pt_{10} clusters on γ-Al_2O_3 have shown that their dynamical structure, and the interplay between charge transfer and entropic effects explain all of the anomalous properties observed by Kang *et al.*[32] in these systems.

Some previous DFT/MD simulations have been carried out on C-supported nanoclusters; however, these systems do not exhibit the structural anomalies like those on γ-Al_2O_3.[158] More recently, in related work on Pt-Sn alloys,[151] it was

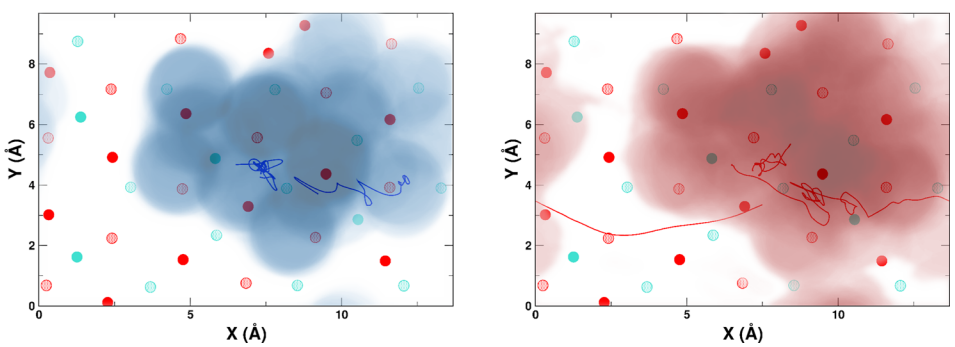

FIG. 10. (Color online) Trajectories of the center of mass (full lines) and cluster footprint (fuzzy shading) projected onto the support, at 165 K (left) and 573 K (right) for Pt_{10} nanoparticles on γ-Al_2O_3. The circles indicate the positions of the O and Al atoms with full circles corresponding to O atoms in the top support layer and shaded ones to the second layer. The trajectories show the 1–2 Å amplitude "rattle" motion of the clusters as well as long "roll" events, especially at higher temperature. The intensity of the footprint indicates that the clusters have a tendency to remain in certain areas of the support, and that at higher temperature the area of contact is notably larger.

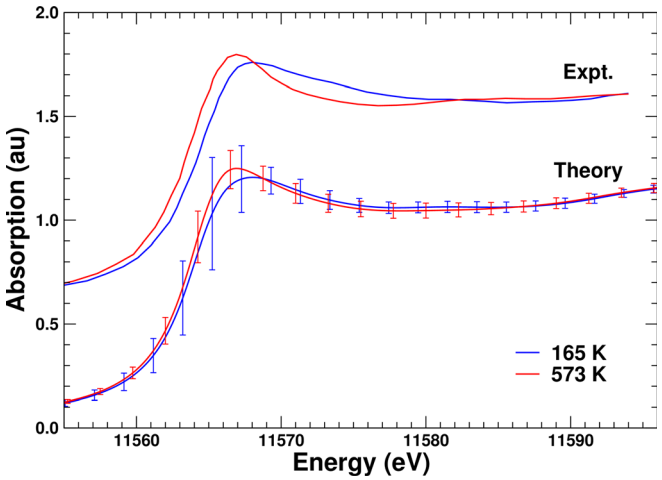

FIG. 11. (Color online) Experimental and theoretical Pt L_3 edge XANES of Pt nanoparticles on γ-Al_2O_3 at 165 and 573 K. The error bars of the theoretical results indicate the standard deviations of the spectra due to the dynamical disorder of the nanoparticles. Adapted with permission from Vila *et al.*, Phys. Rev. B **78**, 121404 (2008). Copyright 2008, American Physical Society.

recognized that this anomalous disorder is largely dynamic in origin and has been characterized as "dynamic structural disorder" (DSD). A significant fraction of this disorder arises not from normal local vibrations or static aperiodic configurations, but from the transient nature of the metallic bonds within the clusters. Thus, the structure of the supported nanoparticles is more characteristic of a quasiliquid than a solid particle, with no well-defined equilibrium structure.

Obviously, surface effects are very important for nanoparticles. By accounting for the dynamic disorder arising from librational motion of the center of mass, the DFT/MD simulations[150] successfully reproduced many of the puzzling behaviors documented in the present (and notable past) work, including NTE and corresponding XANES related electronic effects detailed above. This study emphasized the interrelatedness of these phenomena, providing new and general insights into the dynamics of supported metal nanoparticles. The DFT/MD simulations also reveal that the NTE is directly related to the interaction with the substrate, since the particles show a marked contraction parallel to the support while they expand normal to it. This structural behavior, as dictated by metal-supported charge-transfer, results within the theoretical model in a net and progressive NTE of the average Pt-Pt bond distances. This contraction is particularly noticeable at those Pt atoms that are not in contact with the oxygen atoms of the support, and thus preserve their metallic character. Opposite to the oxidized Pt atoms, which exhibit a positive net charge, the metallic Pt atoms are nearly neutral and thus much more able to accommodate a bond contraction with less Coulomb repulsion. Given that they are not tethered to the surface, the metallic Pt atoms are responsible for the majority of the anomalous disorder. Both this distinct dynamical behavior and differential charging can have implications for the catalytic properties of the nanoparticles. These implications are discussed in more detail in the following sections.

Formally, catalytic properties such as transition rates depend on free energies calculated from equilibrated trajectories or statistical ensembles that contain all accessible regions of configuration space. In practice, however, calculations of adequate ensembles can be impractical, especially for "rough" energy landscapes. Moreover, techniques for characterizing nanoscale structure based on DFT and equilibrium geometries are incomplete, since they typically ignore vibrations and non-equilibrium effects such as bond-breaking and charge fluctuations.

For these reasons finite-temperature dynamic approaches have become increasingly used in recent years.[159,160] The description of dynamic trajectories within DFT makes it possible to go beyond the static description of structure and reactivity, and also to incorporate fluxional (i.e., with dynamically fluctuating bonds) behavior and thermal effects. Quasidynamical approaches have also been introduced to deal with long-time behavior and rare-event sampling.[161–164]

Practical estimates of reaction rates at surfaces can now be carried out with transition state theory and its generalizations, as discussed for example by Jónsson.[165] Reaction paths obtained with the nudged elastic band method are frequently used to estimate reaction rates in the transition state method for surface reactions. The method can also be employed for long time-scale evolution of structure, analogous to the Wigner, Keck, and Eyring two-step procedure, where long-time classical trajectories are replaced by pathways using extensions of the nudged elastic band[166,167] with shifted end-points. It is not yet evident, however, whether such surface science approaches can also be applied to highly disordered nanoparticles at high temperatures.

C. Nanoscale fluctuations

In an effort to understand some of the above difficulties, Rehr and Vila (RV) have proposed a method based on a combination of statistical mechanics and DFT/MD simulations.[152] As noted above, the DFT/MD approach naturally treats DSD effects at high temperatures, since it builds in anharmonic and structural disorder. Such methods can also be directly compared to experiment, since observable physical properties are typically expressed by averages over a statistical ensemble, which are equivalent to time averages over sufficiently long intervals that cover the accessible phase space.

As emphasized by RV, the thermal properties of nanostructures with relatively small numbers of particles N of the order of 10–100 differ substantially from those in macroscopic systems. Even if the entire system (nanostructure plus support) is in thermal equilibrium, the internal temperature of the nanostructures will exhibit fluctuations of order $T/\sqrt{N}$.[168] This can be important for catalysis since the fluctuating local temperature of the nanoparticle rather than the equilibrium temperature T is important for reaction rates, which vary exponentially with the local temperature. The statistical arguments can be summarized as follows: Consider, for example, a nanoparticle with N atoms in contact with a support at a fixed temperature T. Due to contact with the support, which is in continuous thermal motion,

energy will fluctuate between the cluster and the support with a probability distribution

$$\mathrm{P(E;}\beta) \approx e^{S(E)/k-\beta\cdot E}. \quad (3)$$

Here, E is the total energy of the cluster and $S(E) = k \ln \Omega(E)$ is the cluster entropy due to distinguishable configurations $\Omega(E)$. At the equilibrium point, $P(E;\beta)$ is a maximum as a function of energy E, $P(E) = \exp(-\beta F)$, where $F(T) = E - TS$ is by definition the Helmholtz free energy. The mean total cluster energy $\bar{E}$ is then related to the temperature of the support by the relation $dE = TdS$ so that $\partial S/\partial E = 1/T$, and hence, the mean energy per particle in the nanoclusters is consistent with thermal equilibrium. Remarkably, however, the nanoparticles exhibit large temperature fluctuations and hence large deviations from thermal equilibrium. While $P(E)$ is sharply peaked it has an approximately Gaussian shape, and the mean squared fluctuations in the energy are related to the 2nd derivative of the entropy $\sigma_E^2 = k/[\partial^2 S(E)/\partial E^2]$. These fluctuations are order of N and given by $\sigma_E \propto kT\sqrt{3N}$, and since the total energy $E = 3NkT$ from the equipartition theorem, the fluctuations in temperature are $\sigma_T = T/\sqrt{3N}$. For example, the internal temperature distribution of the nanoparticles at T = 600 K has a width of 75–100 K for clusters of 10–20 atoms. As discussed by RV, the nature of the fluctuations can be understood using a coupled oscillator model that includes center of mass motion. The dominant modes include both bond vibrations and slow (sub THz) librational modes. The contributions from the librational modes of the center of mass (CM) in the $x-y$ plane with kinetic energy $(1/2)MV_{lib}^2 = kT$ give rise to a stochastic CM motion, which induces large fluctuations in structure. This rattle motion is the analog of Brownian motion hindered by the substrate bonds. Similar thermodynamic arguments also explain the large charge fluctuations in the nanoparticles.

D. Implications for catalysis

The above summary for supported Pt nanoclusters[150,151] suggests that a DFT/MD approach that accounts for their fluctuating bonding and electronic structure may provide an important prerequisite to a better understanding of their catalytic activity. In particular, the internal fluctuations lead to a larger statistical ensemble of configurations than would be probed at fixed cluster energy.[169,170] Therefore, dynamical, real-time methods make it possible to simulate the statistical ensemble of possible reaction sites. Surface effects are also important and differ from those of the internal structure. Thus, it has been suggested[151] that the surface structure and dynamics can be more important than the global average morphology of clusters. Since experimental probes generally measure global averages, there are two major opportunities for advancing the characterization of the catalytically active systems, and better integrate experiment and theory. For the former, it is important to complement average information ascertained through conventional absorption and scattering techniques, with local studies that provide statistical information. For the latter, it is important in the theoretical analysis to differentiate between surface and internal structures.

The importance of heterogeneous and dynamical structure for catalytic behavior has also been proposed to understand enzyme catalysts in biochemistry. For example, protein dynamic motion has been employed by Schramm *et al.*[171] to account for catalysis, without requiring the tight-binding transition state model of Pauling. In their model, the catalytic activity of a metalloprotein has been attributed to the combination of fast dynamics of the active site and slow dynamics of the protein backbone. Together, the enzyme can explore a larger portion of phase space than if it were only due to the active site dynamics. These structural effects can also play a role in heterogeneous catalysis. For example, the highly flexible local environment around the reaction substrate has a fairly broad vibrational spectrum. Thus, it has the potential to couple with the reaction mode, rapidly adapt to distortions, and broaden bottlenecks in the reaction channels. In spite of this conformational flexibility, the electronic structure of enzymatic active sites is usually well-defined even in enzymes with metallic centers.[172] In supported Pt and Pt alloy nanoparticles, however, simulations have shown that the local electronic structure of the binding sites is highly heterogeneous. For instance, the oxidation state of a Pt atom varies significantly depending on its local environment.[150] Thus, the dynamical disorder in these systems effectively induces a myriad of possible active sites. In typical reactions such as CO dissociation, the reaction is initiated by a weakening of the CO bond induced by the adsorption on a Pt atom.[173] This weakening is coupled to the oxidation state of the Pt atom and thus is expected to be strongly affected by dynamical effects.

IV. ELECTRON MICROSCOPY

A. Introduction

Most spectroscopic and scattering methods suffer from ensemble averaging effects that serve to limit the interpretation of the results.[174,175] It is for this reason that in addition to the quantitative measurements of structure and dynamics of an "average" particle in the ensemble afforded by bulk techniques such as XAS, a local probe is required, capable of measuring the distribution of catalyst particle sizes, shapes, order (e.g., strain, faceting, twinning, dislocations, or other defects), and elemental composition. Transmission electron microscopy (TEM) and scanning transmission electron microscopy (STEM) are extremely well-suited for this purpose.[176,177] This information is accessible by x-ray spectroscopy only indirectly—via sophisticated modeling—and it is easy to overlook such details or misinterpret them. For example, surface disorder in nanoclusters can be mistaken for a reduction in size.[178] A broad intraparticle compositional distribution can also lead to an incorrect assignment of the compositional motif as "core–shell" even though each nanoparticle may be a perfectly random alloy.[175] Hence, in addition to the average information provided by XAS and other bulk probes, a local structural probe that provides

statistical analysis of sizes, degrees of order, crystalline structure, and morphologies is vitally important. The greatest impact, though, comes when such information needs to be explicitly correlated with the average measurements that, in the case of supported metal catalysts, are more and more often done as *in situ* or *operando* measurements. In this section, we will review the recent developments which are credited for providing significant improvements of the spatial and spectral resolution of electron microscopy characterization of catalysts.

The development of aberration (C_s) correction has dramatically improved the spatial resolution of the electron microscope (Fig. 12) even when using lower accelerating voltages.[179] This is particularly advantageous, since a lower accelerating voltage generally leads to less sample damage from the electron beam. Researchers have begun exploiting the capabilities of aberration corrected electron microscopes for the characterization of nanocrystal morphologies. These measurements provide explicit depictions of the atomic structural attributes of heterogeneous catalytic materials.

B. Scanning transmission electron microscopy

The conventional use of high angle annular dark field (HAADF)-STEM allows probing of the microstructures of catalytic materials with a resolution of a few ångströms.[176] This method works by focusing the electron beam to a small point and rastering it across the area of interest. Instead of measuring interference effects created when electrons transit the sample, HAADF-STEM relies on the detection of electrons scattered at high angles relative to the transmitted beam (Rutherford scattering) using an annular detector.[177,180] The image contrast remains strongly dependent on Z,[181] which provides the foundation for so-called "Z-contrast" imaging—a technique that allows high-contrast imaging of high-Z elements (such as the metal in a heterogeneous catalyst) against the background of a low-Z material (such as a support).[182] The addition of C_s-correctors and monochromators to dedicated STEM instruments permits atomic level Z-contrast imaging coupled with regionally selective spectroscopy. When viewing structures even a few nanometers in dimension with C_s-STEM, it is possible to distinguish individual atoms, columns and/or regions containing elemental enrichment.

One exemplary work that expanded upon the aforementioned capabilities of C_s-STEM for the characterization of bimetallic catalysts is the work by Sanchez *et al.*[183] In their work, a series of controlled, monometallic and bimetallic structures were synthesized using controlled methodologies and characterized using C_s-STEM: Pt-Pd core–shell [Fig. 13(a)], Pd-Pt core–shell [Fig. 13(b)], and Pt-Pd alloy clusters [Fig. 13(c)]. In addition to direct inspection of the images and using line scan intensities, the authors used Fourier transforms of the micrographs [Figs. 13(d)–13(f)], STEM simulations, a novel atom counting technique, and energy dispersive x-ray spectroscopy to interpret the observed structures. The use of an image's Fourier transform (power

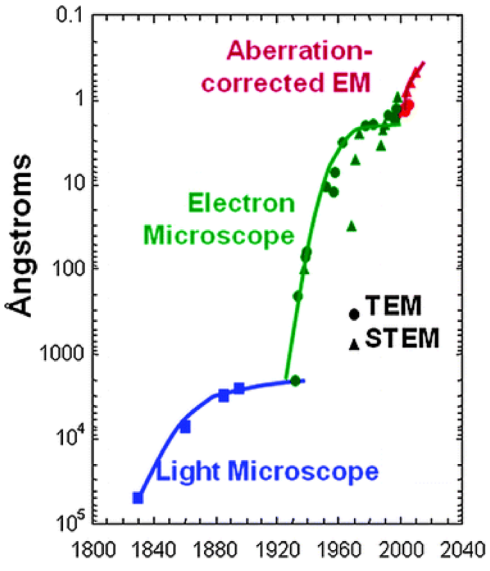

FIG. 12. (Color online) Development of the spatial resolution of optical and electron microscopes. The current rapid improvement in resolution is due to the development of aberration correctors for the electromagnetic lenses, with the current best point-to-point spatial resolution of 0.5 Å (Ref. 179).

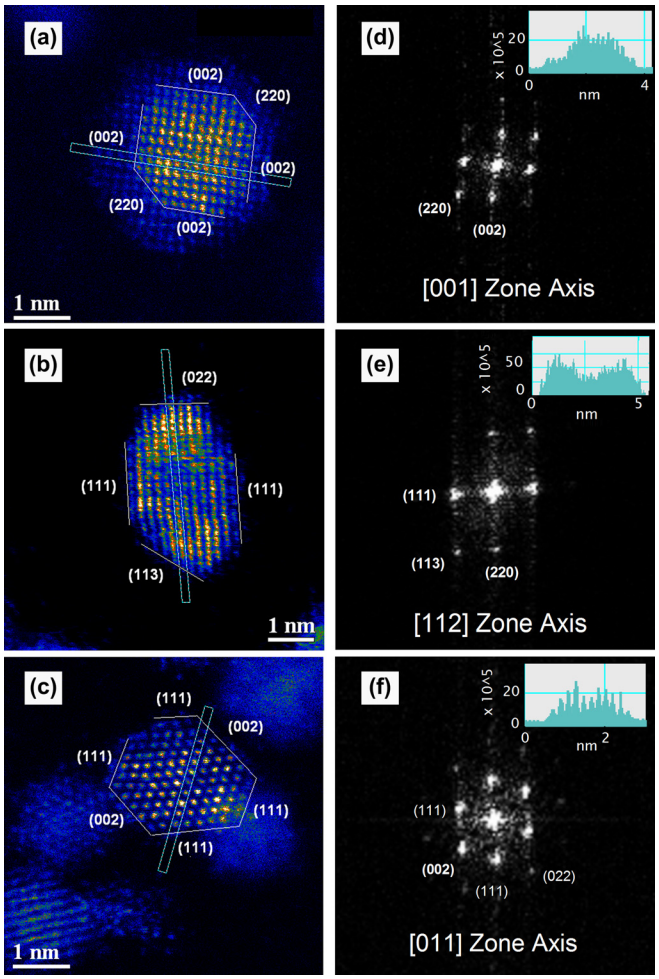

FIG. 13. (Color online) C_s-corrected HAADF STEM images of Pd-Pt nanoparticles. Image of (a) a Pt(core)-Pd(shell), (b) a Pd(core)-Pt(shell), and (c) a coreduced Pt/Pd nanoparticle with labeled crystal facets and the areal integrated intensity measurement made within the boxed region. Corresponding power spectrum data and integrated intensity profile measurement shown as the inset in (d-f). Adapted with permission from Sanchez *et al.*, J. Am. Chem. Soc. **131**, 8683 (2009). Copyright 2009, American Chemical Society.

spectrum) is advantageous, because it is in essence a diffraction pattern of the 2D projection of the system being analyzed.

C. *In situ* electron microscopy

Aberration-corrected transmission electron microscopy is a remarkably powerful tool to determine internal structure and chemical composition at the atomic scale. As recent developments of the XAS technique demonstrate, the rapidly advancing state of the art in studying catalytic processes experimentally is highlighting the use of *in situ* or *operando* methods. X-ray absorption and scattering (e.g., high energy XRD pair distribution function[184,185]) techniques gain fundamental understanding of the structure–catalytic properties of the supported nanoparticles by characterizing them under the appropriate environmental conditions. *In situ* and *operando* results are frequently quite different from static, pre- or post-reaction observations because they provide valuable information and are therefore much more appropriate for studies of mechanisms of catalytic reactions.[81,134,186–189] As discussed above, theoretical developments are also progressing toward *in operando* modeling. One way to study working catalysts by "environmental" TEM (ETEM) is by using observations of the sample during exposure to an external stimulus such as gas or liquid environments, nanoindentation, tensile strain, temperature, radiation, or electric or magnetic fields.[88,190–243] Recent development revealed ETEM as an exciting tool, capable of providing unique information on the structural properties/dynamic processes relationships of nanomaterials. Of particular interest are the structural changes occurring under "real" environmental conditions observable by ETEM. The ETEM allows dynamic studies and development of a fundamental, atomic-level understanding of chemical reactions such as catalysis,[195–197,203,204,206,230] oxidation,[201,212–220,222,225,228] and nanoprocessing.[192,194,202,203,207–211,225–227,238]

At the heart of the ETEM's capabilities is its ability of imaging with gas pressures in the sample chamber as high as 1 atmosphere or even in liquid environments.[244] In contrast, conventional TEMs require high-vacuum conditions with pressure levels on the order of 10^{-6} Torr. Two methods currently exist to transform a TEM into an ETEM. The first is to use differential pumping so that a gas may be introduced into the specimen region while maintaining high vacuum conditions near the electron gun, with gas pressures reaching levels of the order of 10 Torr. This approach has the advantage that the full resolution and analytical capabilities of the instrument can be maintained, if gas pressures do not exceed ~10 Torr.[245] The second method is to use specialized TEM sample holders possessing ultrathin, electron transparent membranes to contain the gas and/or the liquid.[246,247] This approach allows measurements at super-atmospheric pressures, but at the cost of resolution and analytic functionality. The two approaches are in fact quite complementary, in that it is possible to combine both to determine functionality at atmospheric pressure and to confirm that lower pressure/higher resolution measurements maintain their validity.

In situ high resolution TEM (HRTEM) is ideal for characterizing the morphology, crystallinity, and defect structure of individual nanoparticles and their changes under environmental conditions. This information is frequently combined with electron diffraction.[248] Statistical information about these characteristics can be provided as well. An elegant example of observing morphological changes *in situ* was given by Hansen *et al.*, where surface faceting was observed by HRTEM of a Cu nanoparticle supported on ZnO during various gas exposures at 220 °C.[193] The image shown in Fig. 14(a) was taken under H_2 (1.5 mbar). In comparison, Fig. 14(b) was obtained during exposure to a gas mixture of H_2 and H_2O (3:1, 1.5 mbar total pressure). Finally, Fig. 14(c) shows the same cluster after exposure to a gas mixture of H_2

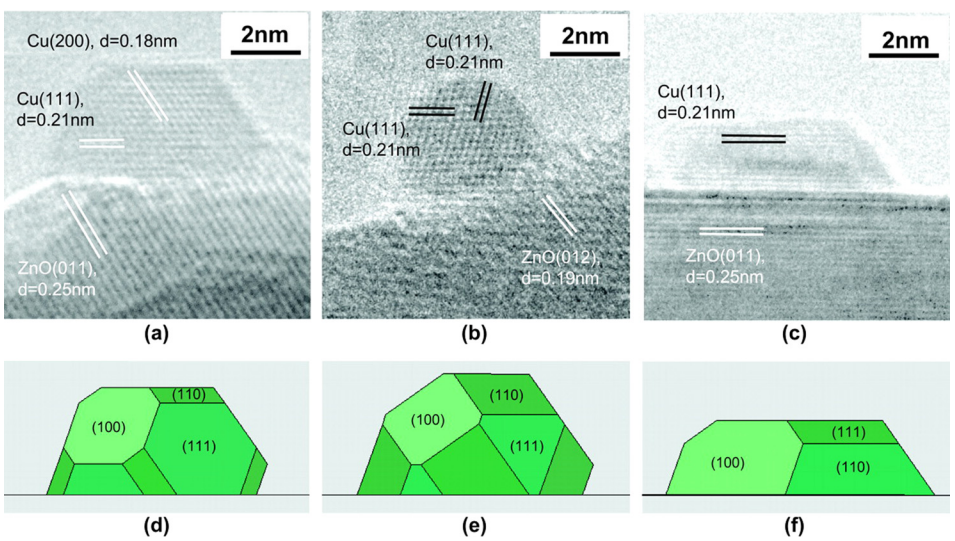

FIG. 14. (Color online) Surface faceting of a Cu nanoparticle supported on ZnO in various gas environments [(a), (d) pure H_2; (b), (e) a mixture of H_2:H_2O = 3:1; and (c), (f) a mixture of 95% H_2 and 5% CO], where (a), (b), and (c) are *in situ* HREM images and (d), (e), and (f) are the corresponding Wulff constructions. The data were measured under a total pressure of 1.5 mbar (a), (b), (d), (e) or 5 mbar (c), (f), respectively, and a temperature of 220 °C. Adapted with permission from Hansen *et al.*, Science **295**, 2053 (2002), Copyright 2002, AAAS.

and CO (95%:5%, 5 mbar total pressure). The corresponding Wulff constructions for each structure are shown in Figs. 14(d)–14(f).[193] This seminal work demonstrated that nanocharacterization under environmental conditions is necessary to gain insights into structure-catalytic property relationships because the morphology of the nanoparticle is quite sensitive to its environment. The specifics of this work also exemplify the type of information obtainable by *in situ* HRTEM including: (1) the relative orientation between the nanoparticle and the support (Hansen *et al*. deduced a weak interfacial bond) and (2) Wulff reconstruction of the 3D shape (and the corresponding facets), which may provide critical information on the surface and interface energies under different gas atmospheres.[249]

Recently, Yoshida *et al*. reported imaging of the surface reconstruction of Au clusters due to CO exposure using aberration-corrected ETEM.[91] They investigated Au/CeO_2 catalysts that are of interest because of their high activity for CO oxidation at room temperature. During exposure to CO they observed changes to the Au(100) facets (Fig. 15) and using image simulations, they determined that the CO was adsorbed on the top sites of the reconstructed Au surface. This work demonstrates the remarkable ability of ETEM to detect structural features due to both the catalyst and the adsorbate bonding under environmental conditions at an atomic level.[91]

A more recent idea in ETEM is to use electron energy loss spectroscopy (EELS) to analyze not the particles within the system, but the products being formed in a catalytic reaction. In the work by Crozier *et al*., EELS was combined with a differentially pumped ETEM under ~1–3 Torr of gas.[250] They showed that standard EELS analysis is not adequate because inelastic scattering along the entire gas path length

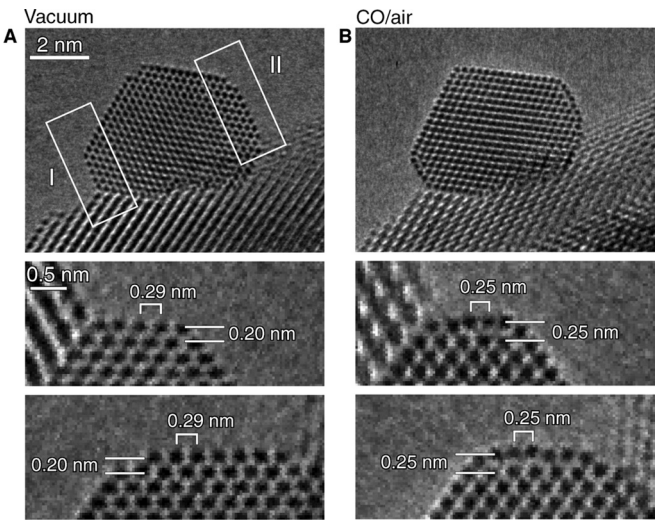

FIG. 15. Au nanoparticles supported on CeO_2 in (a) vacuum and (b) 1 volume% CO in air at 45 Pa and room temperature. Two (100) facets are indicated by I and II in (a). The enlarged images of these regions in vacuum and in the CO/air mixture are shown at the bottom of (a) and (b), respectively, revealing changes in the distance between the first and the second (100) surface layers as well as the (200) planes in crystalline bulk gold. These changes in positions of the Au atomic columns correspond well to those of the Au (100) reconstructed surface structure. Reproduced with permission from Yoshida *et al*., Science **335**, 317 (2012). Copyright 2012, AAAS.

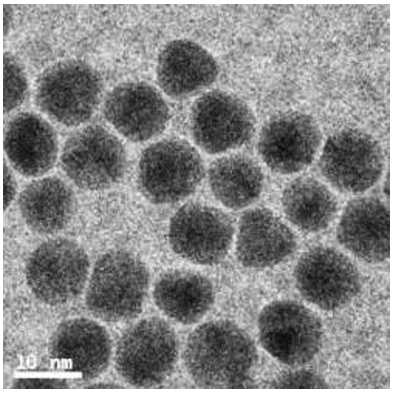

FIG. 16. Bright field TEM images of Au nanoparticles in N_2 (1.1 atm) taken on an FEI Titan at 300 kV using an *in situ* TEM gas flow specimen holder by Hummingbird Scientific.

(particularly when this distance approaches the size of the pole-piece gap) leads to substantially different scattering than from a thin film. Nonetheless, it is possible to reduce the error of quantitative detection of inelastic scattering by using small convergence and collection semiangles when acquiring the spectra. This makes it possible to identify the concentration of different species in the gas with an accuracy better than 15% and creates the possibility of monitoring mass transport during catalytic reactions.

ETEM has provided a wealth of critical information on morphology changes, elemental distributions, and valence states under environmental conditions. There remain limitations given that current commercially available ETEMs based on differential pumping have maximum pressures in the range of some 10^{-2} Torr. Yet catalytic operating environments may be well over 1 atm. To achieve the higher pressures required for *operando* studies, several companies are developing ETEM holders that permit heating and gas pressures up to 1 atm.[251–253] A major engineering challenge for environmental holders is their stability, i.e., the image must remain stable for HRTEM or elemental acquisition, while being heated (thermal drift) or exposed to gas flow. Recent results from Hummingbird Scientific (among others) have demonstrated imaging capabilities at 1.1 atm (Fig. 16). It should also be noted that liquid cell TEM sample holders are already commercially available. Liquid sample cells have been used recently to examine nanoparticle growth and self-assembly.[254] It should also be noted that specialized TEM holders capable for photoexcitation (useful for photocatalysis studies) are also currently being developed.[255]

D. Potential and limitations

Electron microscopy is a local characterization technique that uses electrons to probe a sample. The two primary limitations of electron microscopy are the effects of beam damage and the amount of data that is needed to be representative of a more complex heterogeneous sample. Concerning radiation effects, the sample damage could be due to knock-on or ionization mechanisms. Specht *et al*. using an aberration-corrected TEM with tuneable

accelerating voltage between 80 and 300 keV showed that the structure of the nanoparticles changes depending on the accelerating voltage, with higher voltages leading to more faceted nanoparticles.[256] This phenomenon may be due to the energy of the electrons allowing the atoms to become more mobile, i.e., to move to more energetically favorable (faceted) sites. An additional adverse effect is the possibility to misinterpret the measurement when the sample may indeed change, e.g., upon a chemical reaction or changes in temperature or pressure. These effects are the main objective of ETEM investigations of catalytic reaction mechanisms, and, therefore, special care is needed to minimize the artifacts arising from radiation damage.

One direction to follow toward this goal is to combine the results of electron microscopy with those obtained by average methods, notably XAS. The data from such experiments complement each other's sensitivities to different aspects of atomic structural and electronic attributes and thus in conjoined form provide a more complete assessment of the materials' features. For example, although XAS is a remarkable nanocharacterization tool with characteristics in some critical regards superior to TEM, notably in terms of average spatial resolution, spectral resolution, and capability of detecting adsorbates (e.g., XAS is capable of determining bond distances with 0.001 Å accuracy and can identify metal–adsorbate bonding), it is an ensemble tool and structural refinement most often relies on the assumption of monodispersity. This assumption needs to be verified using a more localized technique like (S)TEM. One obvious advantage of the XAS-(S)TEM synergy is that it offers an opportunity to better understand heterogeneous systems that may contain particles of different sizes, compositions, and chemical states of the same catalyst.[129,136,257] Another advantage is that they provide a more complete information about the structure and morphology than the individual techniques.[118,128–130,132,258,259] The combination of a local probe, such as TEM, with an ensemble averaging technique, such as XAS, has proven to be exceptionally powerful in revealing how structural defects, strain, adsorbates and temperature alter catalysts.[260] In another recent work, it was shown that the non-crystalline-to-crystalline transition of supported Pt nanoparticles in the subnanometer to nanometer size range is statistical in nature, and strongly affected by particle size, support, and adsorbates.[261] Observations of >3000 particles by HRTEM show a non-crystalline-to-crystalline transition zone that is nonabrupt—there is a size regime where disordered and ordered nanoparticles (NPs) coexist. The NP size at which this transition occurs is strongly dependent on both the adsorbate and the support, and this effect is general for late 5d transition metals. This latest example proves that statistical description of particle–support–adsorbate interactions is needed to account for the contribution of different structures and states of order in nanometer-size supported metal catalysts.

V. FUTURE DIRECTIONS

This review describes the advances in three main techniques that successfully probe complex structure and dynamics of the nanocatalysts: two experimental (XAS and (S)TEM) and one based on theoretical simulations. One of the major goals for the catalysis community is to be able to look at the exact same catalytic material with multiple advanced techniques in order to unravel the complex structure–property relationships. Experimental methodology used in catalytic experiments underwent a paradigm shift in the 1980s, dating back to the work of Clausen *et al.*,[262] who first proposed to combine x-ray absorption spectroscopy and x-ray diffraction measurements of a working catalyst in real time. Combining several complementary techniques in a single experiment allows to capture mutual influences of catalyst attributes on each other as well as on the cluster properties, including its catalytic activity, whereas separate measurements of different effects done at different facilities and with different samples will overlook such correlations.[101] Several authors have further enhanced the combined measurements by adding complementary electronic and vibrational spectroscopy techniques, including ultraviolet-visible (UV/VIS), infrared (IR), and Raman spectroscopy, to the well-established XAS-XRD combination.[72,103,263–267] Weckhuysen *et al.* have combined small and wide angle scattering (SAXS and WAXS) techniques with quick-scanning EXAFS (QEXAFS) to study processes *in situ*.[264,268] Newton *et al.* and later other groups have begun to explore the analytical power of the combinations of diffuse reflectance infrared Fourier transform spectroscopy with time-resolved XAS,[269–272] and time-resolved XRD.[273] Newton and Chupas have advanced the XRD pair distribution function methods for *in situ* and *operando* catalysis studies.[184,185] More details about some of these advances can be found in recent reviews.[101,274]

Although the idea to measure TEM and EXAFS data *in operando* under identical pressure and temperature conditions on the same sample may sound utopian without installing an environmental TEM at the endstation of a synchrotron beamline (a remote possibility, although discussions toward that goal have recently begun), we will propose a much more practical path toward implementing this plan. Current efforts are most universally aimed at combining different techniques in a single experiment *in situ* or *in operando*. This approach is naturally limited by a relatively small number of probes that can be combined in the same experiment. The paradigm shift we propose is to investigate catalytic systems *in operando* by multiple techniques performed in a truly portable *operando* cell that is made compatible with most relevant probes. As an illustration of this approach, we mention here a work by de Groot *et al.*, who carried out an *in situ* scanning transmission x-ray microscopy study of a Fischer-Tropsch catalyst in an enclosed cell with SiN windows.[275] One particular aspect of this work that is appealing to our approach is that the nanoreactor used by de Groot *et al.* was adapted from the cell originally used for high-resolution electron microscopy, and thus remained compatible for application with both x-ray and electron probes.

The benefit of a portable environmental cell is that the exact same samples and environments can be characterized by a large number of complementary methods. This

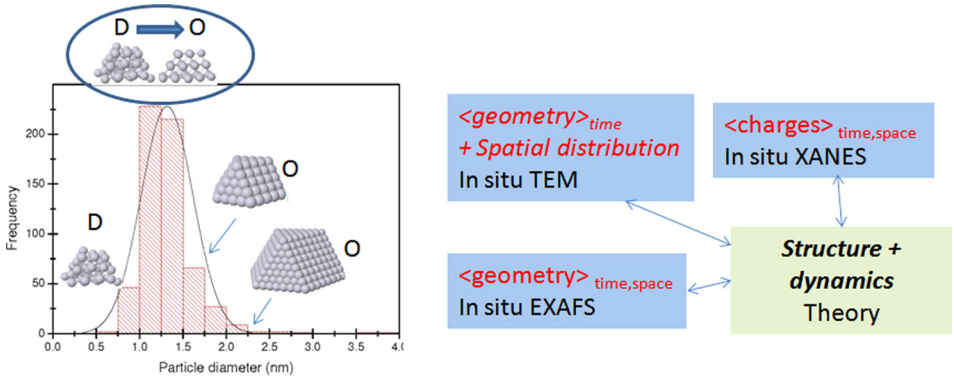

FIG. 17. (Color online) Typical size distribution histogram obtained by TEM for model systems of supported metal clusters. The distribution symbolizes a collection of different structural motifs in real catalytic systems. Shown are cartoons of ordered and disordered clusters that will be observed in each size range. Note the expected transition zone between 1 and 1.5 nm: the ordered (O) and disordered (D) clusters are known to coexist in this range. The chart on the right shows our proposed new investigation method of heterogeneous catalysts: Distributions of particle sizes and compositions will be obtained by *in situ* TEM. Theoretical thermodynamic properties will be calculated for each type of cluster in the distribution and averaged with the experimentally measured distribution. XAS studies of the average pressure and temperatures under which the catalyst operates will be used to validate the theoretical calculations.

approach will remove ambiguities introduced by examining different specimens and/or using different gasses, very limited sample materials can be preserved, and the specimen is protected from the air environment during transfer from one characterization tool to another. The portable cell allows for multiple complementary and necessary tools to characterize catalysts *in operando* conditions.

Multiple experiments performed *in operando* using the portable cell have a unique advantage over the conventional methods used to date. First, the comparison of local and average methods (such as TEM and XAFS, respectively) will allow one to validate, and improve the theory, hence, providing a feedback loop where the experiment and theory are used iteratively. Local measurements by electron microscopy will inform theory on the distribution of different inequivalent cluster forms (Fig. 17). The weighted average of different theoretical simulations obtained for each cluster type using the measured distribution can be then directly compared with the experimentally measured, ensemble-average data by x-ray absorption. In the end, these calculations will allow to both explain and predict the properties of real catalytic systems and account for many of the heterogeneities they embed.

This new analysis scheme is yet to be validated, but the steps in this direction are taken at several synchrotron facilities using different portable cell designs. These efforts will inevitably bring new details, and yet new challenges, on resolving the complex interactions in model and real catalysts.

ACKNOWLEDGMENT

The authors acknowledge the support of this work by the U.S. DOE Grant No. DE-FG02-03ER15476.

[1]A. Gutteridge and J. M. Thornton, Trends Biochem. Sci. **30**, 622 (2005).
[2]P. Arnold, *Origin and History of Beer and Brewing from Prehistoric Times to the Beginning of Brewing Science and Technology* (Alumni Assn. of the Wahl-Henius Institute, Chicago, 1911), p. 411.
[3]M. Faraday, Philos. Trans. R. Soc. Lond. **44**, 77 (1834).
[4]G. B. Kauffman, Platinum Met. Rev. **43**, 122 (1999).
[5]L. J. Thénard, Ann. Chim. Phys. **8**, 306 (1818).
[6]J. J. Berzelius, *Årsberättelsen om framsteg i fysik och kemi*, (Nabu Press of Charleston, SC, 2011).
[7]L. Wilhelmy, Ann. Phys Chem. **81**, 499 (1850).
[8]P. Waage and C. M. Guldberg, *Studies Concerning Affinity. Forhandlinger: Videnskabs - Selskabet i Christinia* (Norwegian Academy of Science and Letters, 1864), Vol. 35.
[9]S. Arrhenius, Z. Phys. Chem. **4**, 226 (1889).
[10]D. L. Chapman, Philos. Mag. **47**, 90 (1899).
[11]I. Langmuir, J. Am. Chem. Soc. **40**, 1361 (1918).
[12]C. Hinshelwood, *Kinetics of Chemical Change* (Oxford Univ. Press, Oxford, 1940).
[13]M. G. Evans and M. Polanyi, Trans. Farad. Soc. **31**, 875 (1935).
[14]P. Sabatier, *La Catalyse en chimie organique* (C. Beranger, Paris, 1913).
[15]F. Haber and G. v. Oordt, Z. Anorg. Chem. **44**, 341 (1905).
[16]F. Haber and R. L. Rossignol, Z. Electrochem. **14**, 181 (1908).
[17]F. Fischer and H. Tropsch, Brennst. Chem. **4**, 276 (1923).
[18]G. Ertl, H. Knözinger, and J. Weitkamp, *Handbook of Heterogeneous Catalysis* (Wiley, New York, 1999).
[19]J. Hagen, *Industrial Catalysis: A Practical Approach*, 2nd ed. (Wiley-VCH, Germany, 2005).
[20]K. Ziegler, German Patent 883067, 1953.
[21]C. D. Keith and J. J. Mooney, U.S. patent 3,896,616, 1975.
[22]C. D. Keith, T. Schreuders, and C. E. Cunningham, U.S. patent 3,441,381, 1969.
[23]I. Chorkendorff and J. W. Niemantsverdriet, *Concepts of Modern Catalysis and Kinetics*, 2nd ed. (Wiley, New York, 2007), 477 pp.
[24]S. Schauermann *et al.*, Acc. Chem. Res. **46**, 1673 (2013).
[25]B. R. Cuenya, Thin Solid Films **518**, 3127 (2010).
[26]M. W. Small *et al.*, ACS Nano **6**, 5583 (2012).
[27]E. C. Marques *et al.*, J. Chem. Phys. **77**, 1027 (1982).
[28]R. Narayanan and M. A. El-Sayed, Nano Lett. **4**, 1343 (2004).
[29]S. Mostafa *et al.*, J. Am. Chem. Soc. **132**, 15714 (2010).
[30]A.-X. Yin *et al.*, J. Am. Chem. Soc. **133**, 3816 (2011).
[31]S. I. Sanchez *et al.*, J. Am. Chem. Soc. **131**, 7040 (2009).
[32]J. H. Kang *et al.*, J. Am. Chem. Soc. **128**, 12068 (2006).
[33]M. W. Small *et al.*, J. Am. Chem. Soc. **133**, 3582 (2011).
[34]C. T. Campbell, Nat. Chem. **4**, 597 (2012).
[35]J. A. Rodriguez *et al.*, Angew. Chem., Int. Ed. **46**, 1329 (2007).
[36]V. Johanek *et al.*, J. Phys. Chem. B **108**, 14244 (2004).
[37]S. Takakusagi *et al.*, Langmuir **26**, 16392 (2010).
[38]W. Zhou *et al.*, Appl. Catal. B **46**, 273 (2003).
[39]E. P. Maris *et al.*, J. Catal. **251**, 281 (2007).
[40]A. L. Marsh, F. H. Ribeiro, and G. A. Somorjai, *Single Crystal Surfaces. Handbook of Heterogeneous Catalysis* (Wiley-VCH, Germany, 2008), Vol. 4, p. 28.
[41]H.-J. Freund, Top. Catal. **48**, 137 (2008).
[42]G. Ertl, Surf. Sci. **6**, 208 (1967).

[43]G. Ertl, Z. Phy. Chem. **46**, 49 (1965).
[44]G. Ertl, *Catalytic Ammonia Synthesis*, edited by J. R. Jennings (Plenum Press, New York, 1991).
[45]B. Lang, R. W. Joyner, and G. A. Somorjai, Surf. Sci. **30**, 440 (1972).
[46]B. Lang, R. W. Joyner, and G. A. Somorjai, Surf. Sci. **30**, 454 (1972).
[47]L. M. Falicov and G. A. Somorjai, Proc. Natl. Acad. Sci. U.S.A. **82**, 2207 (1985).
[48]G. A. Somorjai, K. R. McCrea, and J. Zhu, Top. Catal. **18**, 157 (2002).
[49]R. Imbihl, R. J. Behm, and R. Schloegl, Phys. Chem. Chem. Phys. **9**, 3522 (2007).
[50]R. Schloegl *et al*., Catal. Lett. **1**, 237 (1988).
[51]J. Jortner, Z. Phys. D **24**, 247 (1992).
[52]J. Jortner and C. N. R. Rao, Pure Appl. Chem. **74**, 1491 (2002).
[53]G. Sitja *et al*., Nano Lett. **13**, 1977 (2013).
[54]X. Batlle and A. Labarta, J. Phys. D **35**, R15 (2002).
[55]M. Seidl, K.-H. Meiwesbroer, and M. Brack, J. Chem. Phys. **95**, 1295 (1991).
[56]G. L. Kellogg, Phys. Rev. Lett. **73**, 1833 (1994).
[57]N. Isomura *et al*., J. Vac. Sci. Technol. A **28**, 1141 (2010).
[58]A. S. Worz *et al*., J. Am. Chem. Soc. **125**, 7964 (2003).
[59]J. Kleis *et al*., Catal. Lett. **141**, 1067 (2011).
[60]I. V. Yudanov *et al*., Nano Lett. **12**, 2134 (2012).
[61]C. L. Cleveland and U. Landman, J. Chem. Phys. **94**, 7376 (1991).
[62]D. Schooss *et al*., Philos. Trans. Royal Soc. A **368**, 1211 (2010).
[63]I. S. Atanasov and M. Hou, Solid State Phenom. **172–174**, 670 (2011).
[64]V. N. Parmon, Catal. Today **51**, 435 (1999).
[65]P. W. Atkins, *Physical Chemistry*, 7th ed. (Oxford Univ. Press, Oxford, 2002).
[66]J. Suntivich *et al*. Nat. Chem. **3**, 546 (2011).
[67]B. M. Weckhuysen, Nature **439**, 548 (2006).
[68]A. Tilekaratne *et al*., ACS Catal. **2**, 2259 (2012).
[69]G. Nurk *et al*., J. Power Sources **240**, 448 (2013).
[70]H. Topsøe, J. Catal. **216**, 155 (2003).
[71]J. A. Rodriguez *et al*., Phys. Chem. Chem. Phys. **15**, 12004 (2013).
[72]A. Patlolla *et al*., ACS Catal. **2**, 2216 (2012).
[73]M. G. Weir *et al*., Chem. Phys. Chem. **11**, 2942 (2010).
[74]F. Tao, Chem. Cat. Chem. **4**, 583 (2012).
[75]S. J. Kweskin *et al*., ACS Catal. **2**, 2377 (2012).
[76]J. C. Fierro-Gonzalez, J. Guzman, and B. C. Gates, Top. Catal. **44**, 103 (2007).
[77]X. Nie *et al*., ACS Nano **6**, 6014 (2012).
[78]C. Louis, C. Lepetit, and M. Che, Mol. Eng. **4**, 3 (1994).
[79]K. Shimizu *et al*., J. Phys. Chem. C **111**, 1683 (2007).
[80]M. Høj, A. D. Jensen, and J.-D. Grunwald, Appl. Catal. A **451**, 207 (2013).
[81]E. Stavitski and B. M. Weckhuysen, Chem. Soc. Rev. **39**, 4615 (2010).
[82]G. Rupprechter, Catal. Today **126**, 3 (2007).
[83]A. J. Dent, Top. Catal. **18**, 27 (2002).
[84]T. T. Fister *et al*., Rev. Sci. Instrum. **77**, 063901 (2006).
[85]T. T. Fister *et al*., J. Chem. Phys. **135**, 224513 (2011).
[86]M. Tromp *et al*., AIP Conf. Proc. **882**, 651 (2007).
[87]J. A. v. Bokhoven *et al*., Angew. Chem. Int. Ed. **118**, 4767 (2006).
[88]E. A. Stach *et al*., Philos. Mag. A **80**, 2159 (2000).
[89]F. Cavalca *et al*., Nanotechnology **23**, 075705 (2012).
[90]N. de Jonge *et al*., Proc. Natl. Acad. Sci. USA **106**, 2159 (2009).
[91]H. Yoshida *et al*., Science **335**, 317 (2012).
[92]J. C. Yang *et al*., Chem. Soc. Rev. **41**, 8179 (2012).
[93]S. J. L. Billinge and I. Levin, Science **316**, 561 (2007).
[94]F. Delbecq and P. Sautet, J. Catal. **152**, 217 (1995).
[95]M. Dignea *et al*., J. Catal. **211**, 1 (2002).
[96]M. Dignea *et al*., J. Catal. **226**, 54 (2004).
[97]P. J. Feibelman *et al*., J. Phys. Chem. B **105**, 4018 (2001).
[98]I. Grinberg, Y. Yourdshahyan, and A. M. Rappe, J. Chem. Phys. **117**, 2264 (2002).
[99]R. A. Olsen, P. H. T. Philipsen, and E. J. Baerends, J. Chem. Phys. **119**, 4522 (2003).
[100]S. E. Mason, I. Grinberg, and A. M. Rappe, Phys. Rev. B **69**, 161401 (2004).
[101]A. I. Frenkel, J. A. Rodriguez, and J. G. Chen, ACS Catal. **2**, 2269 (2012).
[102]A. M. Beale *et al*., Chem. Commun. **2005**, 3015.
[103]S. J. Tinnemans *et al*., Catal. Today **113**, 3 (2006).
[104]M. A. Bañares, Catal. Today **100**, 71 (2005).
[105]D. E. Sayers, E. A. Stern, and F. W. Lytle, Phys. Rev. Lett. **27**, 1204 (1971).
[106]S. I. Zabinsky *et al*., Phys. Rev. B **52**, 2995 (1995).
[107]G. Bunker, Nucl. Instrum. Met. **207**, 437 (1983).
[108]J. J. Rehr and R. C. Albers, Rev. Mod. Phys. **72**, 621 (2000).
[109]A. L. Ankudinov *et al*., Phys. Rev. B **58**, 7565 (1998).
[110]J. J. Rehr *et al*., C. R. Phys. **10**, 548 (2009).
[111]S. J. Gurman, N. Binsted, and I. Ross, J. Phys. C **17**, 143 (1984).
[112]A. Filipponi, A. D. Cicco, and C. R. Natoli, Phys. Rev. B **52**, 15122 (1995).
[113]S. R. Bare *et al*., Rev. Sci. Instrum. **77**, 023105 (2006).
[114]S. R. Bare *et al*., Catal. Today **126**, 18 (2007).
[115]E. M. Erickson *et al*., J. Am. Chem. Soc. **134**, 197 (2012).
[116]J. D. Grunwaldt *et al*., Phys. Chem. Chem. Phys. **6**, 3037 (2004).
[117]J. McBreen *et al*., Langmuir **3**, 428 (1987).
[118]M. S. Nashner *et al*., J. Am. Chem. Soc. **119**, 7760 (1997).
[119]K. Sasaki *et al*., Res. Chem. Interm. **32**, 543 (2006).
[120]R. Viswanathan, R. Liu, and E. S. Smotkin, Rev. Sci. Instrum. **73**, 2124 (2002).
[121]R. J. K. Wiltshire *et al*., Electrochim. Acta **50**, 5208 (2005).
[122]Y. Uemura *et al*., Phys. Chem. Chem. Phys. **13**, 15833 (2011).
[123]E. D. Crozier, Nucl. Instrum. Met. Phys. Res. B **133**, 134 (1997).
[124]G. Bunker, *A Practical Guide to X-ray Absorption Fine Structure Spectroscopy* (Cambridge Univ. Press, Cambridge, UK, 2010).
[125]J. A. Penner-Hahn, Coord. Chem. Rev. **190–192**, 1101 (1999).
[126]E. A. Stern and S. M. Heald, *Basic Principles and Applications of EXAFS, in Handbook of Synchrotron Radiation*, edited by E. E. Koch (North-Holland, Amsterdam, 1983), pp. 995–1014.
[127]H. Wende, Rep. Prog. Phys. **67**, 2105 (2004).
[128]A. I. Frenkel, J. Sync. Radiat. **6**, 293 (1999).
[129]A. I. Frenkel, Z. Kristallographie **222**, 605 (2007).
[130]M. S. Nashner *et al*., J. Am. Chem. Soc. **120**, 8093 (1998).
[131]A. I. Frenkel *et al*., Ann. Rev. Anal. Chem. **4**, 23 (2011).
[132]A. I. Frenkel, C. W. Hills, and R. G. Nuzzo, J. Phys. Chem. B **105**, 12689 (2001).
[133]A. E. Russell and A. Rose, Chem. Rev. **104**, 4613 (2004).
[134]J. Singh, C. Lamberti, and J. A. v. Bokhoven, Chem. Soc. Rev. **39**, 4754 (2010).
[135]H. Modrow, Appl. Spec. Rev. **39**, 183 (2004).
[136]A. I. Frenkel, Chem. Soc. Rev. **41**, 8163 (2012).
[137]C. W. Mays, J. S. Vermaak, and D. Kuhlmann-Wilsdorf, Surf. Sci. **12**, 134 (1968).
[138]A. I. Frenkel *et al*., J. Chem. Phys. **123**, 184701 (2005).
[139]J. Rockenberger *et al*., Ber. Bunsenges. Phys. Chem. **101**, 1613 (1997).
[140]R. Xia *et al*., Nanotechnology **21**, 085703 (2010).
[141]A. I. Frenkel *et al*., Phys. Rev. B **85**, 195419 (2012).
[142]J. H. Hodak, A. Henglein, and G. V. Hartland, J. Chem. Phys. **111**, 8613 (1999).
[143]X. Zhou *et al*., J. Am. Chem. Soc. **132**, 138 (2010).
[144]K. P. McKenna and A. L. Shluger, J. Phys. Chem. C **111**, 18848 (2007).
[145]D. R. Rolison, Science **299**, 1698 (2003).
[146]J. V. Barth, G. Costantini, and K. Kern, Nature **437**, 671 (2005).
[147]K. Koga, T. Ikeshoji, and K.-i. Sugawara, Phys. Rev. Lett. **92**, 115507 (2004).
[148]S. H. Joo *et al*., Nat. Mater. **8**, 126 (2009).
[149]A. Groß, Surf. Sci. **500**, 347 (2002).
[150]F. Vila *et al*., Phys. Rev. B **78**, 121404 (2008).
[151]F. D. Vila *et al*., University of Washington Preprint, 2013.
[152]J. J. Rehr and F. Vila, arXiv:1309.1493.
[153]R. Car and M. Parrinello, Phys. Rev. Lett. **55**, 2471 (1985).
[154]F. J. Keil, Multisc, Mol. Methods Appl. Chem. **307**, 69 (2012).
[155]L. L. Wang and D. D. Johnon, J. Am. Chem. Soc. **131**, 14023 (2009).
[156]N. A. Zarkevich and D. D. Johnson, Phys. Rev. Lett. **92**, 255702 (2004).
[157]J. S. Tse, Ann. Rev. Phys. Chem. **53**, 249 (2002).
[158]L. L. Wang and D. D. Johnson, J. Am. Chem. Soc. **129**, 3658 (2007).
[159]K. M. Neyman and F. Illas, Catal. Today **105**, 2 (2005).
[160]P. Sautet and F. Delbecq, Chem. Rev. **110**, 1788 (2010).
[161]A. Laio and M. Parrinello, Proc. Natl. Acad. Sci. U.S.A. **99**, 12562 (2002).
[162]L. Rosso and M. E. Tuckerman, Mol. Simul. **28**, 91 (2002).
[163]M. Sprik and G. Ciccotti, J. Chem. Phys. **109**, 7737 (1998).
[164]A. F. Voter, Phys. Rev. Lett. **78**, 3908 (1997).
[165]H. Jónsson, Proc. Natl. Acad. Sci. U.S.A. **108**, 944 (2011).

[166]G. Henkelman, B. P. Uberuaga, and H. Jonsson, J. Chem. Phys. **113**, 9901 (2000).
[167]G. Henkelman and H. Jonsson, J. Chem. Phys. **113**, 9978 (2000).
[168]L. D. Landau and E. M. Lifshitz, *Statistical Physics*, 3rd ed. (Butterworth-Heinmann, Oxford, 1980).
[169]P. G. Bolhuis *et al.*, Ann. Rev. Phys. Chem. **53**, 291 (2002).
[170]C. Dellago, P. G. Bolhuis, and D. Chandler, J. Chem. Phys. **108**, 9236 (1998).
[171]V. L. Schramm, J. Biol. Chem. **282**, 28297 (2007).
[172]R. H. Holm, P. Kennepohl, and E. I. Solomon, Chem. Rev. **96**, 2239 (1996).
[173]A. D. Allian *et al.*, J. Am. Chem. Soc. **133**, 4498 (2011).
[174]A. I. Frenkel *et al.*, "Complexity of nanoscale atomic clusters," in *Encyclopedia of Complexity and Systems Science*, edited by R. Myers (Springer, New York, 2009), pp. 5889–5912.
[175]A. I. Frenkel *et al.*, J. Chem. Phys. **138**, 064202 (2013).
[176]P. Goodhew, J. Humphreys, and R. Beanland, *Electron Microscopy and Analysis*, 3rd ed. (Taylor & Francis, London, 2001), pp. 76–80.
[177]D. B. Williams and B. C. Carter, *Transmission Electron Microscopy: Basics* (Springer Science+Business Media Inc., New York, 1996).
[178]A. Yevick and A. I. Frenkel, Phys. Rev. B **81**, 115451 (2010).
[179]S. J. Pennycook *et al.*, "Scanning transmission electron microscopy of nanostructures," in *The Oxford Handbook of Nanoscience and Nanotechnology*, edited by A. V. Narlikar and Y. Y. Fu (Oxford Univ. Press, Oxford, United Kingdom, 2010), p. 205.
[180]S. Rosenthal *et al.*, Surf. Sci. Rep. **62**, 111 (2007).
[181]X. Xu *et al.*, Nanotechnology **18**, 225501 (2007).
[182]A. Singhal, J. C. Yang, and J. M. Gibson, Ultramicroscopy **67**, 191 (1997).
[183]S. I. Sanchez *et al.*, J. Am. Chem. Soc. **131**, 8683 (2009).
[184]P. J. Chupas *et al.*, J. Am. Chem. Soc. **129**, 13822 (2007).
[185]M. A. Newton *et al.*, J. Am. Chem. Soc. **134**, 5036 (2012).
[186]G. A. Somorjai and C. Aliaga, Langmuir **26**, 16190 (2010).
[187]S. Surnev, M. G. Ramsey, and F. P. Netzer, J. Phys. **13**, 11305 (2001).
[188]E. Stavitski, A. M. Beale, and B. M. Weckhuysen, "Catalyst characterization—heterogeneous," in *Encyclopedia of Catalysis* (Wiley, New York, 2010), pp. 5–20.
[189]A. M. Beale, S. D. M. Jacques, and B. M. Weckhuysen, Chem. Soc. Rev. **39**, 4656 (2010).
[190]E. A. Stach, Mater. Today **11**, 50 (2008).
[191]P. L. Gai, R. Roper, and M. G. White, Curr. Opin. Solid State Mater. Sci. **6**, 401 (2002).
[192]S. Hofmann *et al.*, J. Phys. Chem. C **113**, 1648 (2009).
[193]P. L. Hansen *et al.*, Science **295**, 2053 (2002).
[194]T. Sun *et al.*, Phys. Rev. B **77**, 205414-1-6 (2008).
[195]S. Alayoglu *et al.*, Nat. Mater. **7**, 333 (2008).
[196]S. Hofmann *et al.*, Nano Lett. **7**, 602 (2007).
[197]R. Wang *et al.*, Nano Lett. **8**, 962 (2008).
[198]R. C. Hugo *et al.*, Acta Mater. **51**, 1937 (2003).
[199]Z. L. Wang, P. Poncharalb, and W. A. d. Heerb, J. Phys. Chem. Solids **61**, 1025 (2000).
[200]D. S. Shih, I. M. Robertson, and H. K. Birnbaum, Acta Met. **36**, 111 (1988).
[201]F. M. Ross and J. M. Gibson, Phys. Rev. Lett. **68**, 1782 (1992).
[202]F. M. Ross, R. M. Tromp, and M. C. Reuter, Science **286**, 1931 (1999).
[203]P. L. Gai, R. Sharma, and F. M. Ross, MRS Bull. **33**, 107 (2008).
[204]P. L. Gai, Adv. Mater. **10**, 1259 (1998).
[205]E. Boyes, P. L. Gai, and L. G. Hanna, MRS Proc. **404**, 53 (1995).
[206]P. L. Gai, Acta Crystallogr., Sect. B: Struct. Sci. **53**, 346 (1997).
[207]A. Portavoce *et al.*, Phys. Rev. B **70**, 195306-1-9 (2004).
[208]J. B. Hannon *et al.* Nature **440**, 69 (2006).
[209]P. C. Searson *et al.*, Surf. Sci. **600**, 1817 (2006).
[210]B. J. Kim *et al.*, Science **322**, 1070 (2008).
[211]C. Wiethoff *et al.*, Nano Lett. **8**, 3065 (2008).
[212]J. C. Yang *et al.*, Scr. Mater. **38**, 1237 (1998).
[213]J. C. Yang *et al.*, Appl. Phys. Lett. **70**, 3522 (1997).
[214]J. C. Yang, L. Tropia, and D. Evan, Appl. Phys. Lett. **81**, 241 (2002).
[215]G. Zhou and J. C. Yang, J. Mater. Res. **20**, 1684 (2005).
[216]G. W. Zhou *et al.*, Appl. Phys. Lett. **93**, 123104 (2008).
[217]G. W. Zhou, W. S. Slaughter, and J. C. Yang, Phys. Rev. Lett. **94**, 246101 (2005).
[218]G. W. Zhou and J. C. Yang, Phys. Rev. Lett. **89**, 106101 (2002).
[219]G. W. Zhou *et al.*, Phys. Rev. Lett. **96**, 226108 (2006).
[220]G. W. Zhou *et al.*, J. Appl. Phys. **101**, 033521 (2007).
[221]M. Yeadon *et al.*, Appl. Phys. Lett. **71**, 1631 (1997).
[222]L. Wang *et al.*, Surf. Sci. **600**, 2372 (2006).
[223]M. Bharadwaj and J. Yang, Scr. Mater. **44**, 2557 (2001).
[224]C. G. Zimmermann *et al.*, Phys. Rev. Lett. **83**, 1163 (1999).
[225]K. A. Dick *et al.*, Nano Lett. **7**, 1817 (2007).
[226]C. Detavernier *et al.*, Nature **426**, 641 (2003).
[227]F. M. Ross, J. Tersoff, and R. M. Tromp, Phys. Rev. Lett. **80**, 984 (1998).
[228]F. M. Ross, J. M. Gibson, and R. D. Twesten, Surf. Sci. **310**, 243 (1994).
[229]R. Sharma, J. Mater. Res. **20**, 1695 (2005).
[230]P. L. Gai *et al.*, MRS Bull. **32**, 1044 (2007).
[231]P. J. Ferreira, K. Mitsuishi, and E. A. Stach, MRS Bull. **33**, 83 (2008).
[232]G. M. Bond, I. M. Robertson, and H. K. Birnbaum, Scr. Metall. **20**, 653 (1986).
[233]I. M. Robertson *et al.*, MRS Bull. **33**, 122 (2008).
[234]D. Angang *et al.*, Nano Lett. **7**, 1308 (2007).
[235]T. L. Daulton *et al.*, Microsc. Microanal. **7**, 470 (2001).
[236]A. L. Neal *et al.*, Appl. Surf. Sci. **202**, 150 (2002).
[237]T. L. Daulton, M. A. Kirk, and L. E. Rehn, J. Nucl. Mater. **276**, 258 (2000).
[238]Y. Wu and P. Yang, J. Am. Chem. Soc. **123**, 3165 (2001).
[239]J. S. Kim *et al.*, Science **321**, 1472 (2008).
[240]S. K. Eswaramoorthy, J. M. Howe, and G. Muralidharan, Science **318**, 1437 (2007).
[241]H. Zheng *et al.*, Science **324**, 1309 (2009).
[242]K. C. Chen *et al.*, Science **321**, 1066 (2008).
[243]X. D. Han *et al.*, Nano Lett. **7**, 452 (2007).
[244]K. Kishita *et al.*, "*In situ* TEM observation of solid-gas reactions," in *Electron Microscopy and Analysis Group Conference* (IOP Publishing, Bristol, England, UK, 2007).
[245]T. W. Hansen and J. B. Wagner, Microsc. Microanal. **18**, 684 (2012).
[246]J. F. Creemer *et al.*, J. Micromech. Syst. **19**, 254 (2010).
[247]M. J. Williamson *et al.*, Nat. Mater. **2**, 532 (2003).
[248]J. Liu, Microsc. Microanal. **10**, 55 (2004).
[249]S. Helveg and P. L. Hansen, Catal. Today **111**, 68 (2006).
[250]P. A. Crozier and S. Chenna, Ultramicroscopy **111**, 177 (2011).
[251]J. H. Kwak *et al.*, Science **325**, 1670 (2009).
[252]L. F. Allard *et al.*, Microsc. Microanal. **15**, 1482 (2009).
[253]D. A. Blom *et al.*, Microsc. Microanal. **12**, 483 (2006).
[254]J. Evans *et al.*, Nano Lett. **11**, 2809 (2011).
[255]P. Deshmukh, P. Fischione, J. Gronsky, "Bridging the gap between the environmental cell (e-cell) holder technology and in situ applications in a (scanning) transmission electron microscope," in *Microscopy and Microanalysis* (Microscopy Society of America, Phoenix, AZ, 2012).
[256]P. Specht *et al.*, Microsc. Microanal. **17**, 1064 (2011).
[257]Y. Sun *et al.*, Langmuir **22**, 807 (2006).
[258]B. R. Cuenya *et al.*, J. Am. Chem. Soc. **132**, 8747 (2010).
[259]A. M. Karim *et al.*, J. Am. Chem. Soc. **131**, 12230 (2009).
[260]J. M. Thomas and J.-C. Hernandez-Garrido, Angew. Chem. Int. Ed. **48**, 3904 (2009).
[261]L. Li *et al.*, J. Am. Chem. Soc. **135**, 13062 (2013).
[262]B. S. Clausen *et al.*, Catal. Lett. **20**, 23 (1993).
[263]B. M. Weckhuysen, Phys. Chem. Chem. Phys. **5**, 4351 (2003).
[264]A. M. Beale *et al.*, J. Am. Chem. Soc. **128**, 12386 (2006).
[265]J. G. Mesu *et al.*, J. Phys. Chem. B **109**, 4042 (2005).
[266]A. Patlolla *et al.*, Top. Catal. **56**, 896 (2013).
[267]M. Tromp *et al.*, Chem. Commun. **2003**, 128.
[268]S. Nikitenko *et al.* J. Sync. Radiat. **15**, 632 (2008).
[269]N. S. Marinkovic, Q. Wang, and A. I. Frenkel, J. Sync. Radiat. **18**, 447 (2011).
[270]M. Newton, Top. Catal. **52**, 1410 (2009).
[271]M. A. Newton *et al.*, Nat. Mater. **6**, 528 (2007).
[272]M. A. Newton *et al.*, Catal. Today **126**, 64 (2007).
[273]M. A. Newton *et al.*, J. Am. Chem. Soc. **132**, 4540 (2010).
[274]U. Bentrup, Chem. Soc. Rev. **39**, 4718 (2010).
[275]E. d. Smit *et al.*, Nature **456**, 222 (2008).